Inositol pyrophosphates promote the interaction of SPX domains with the coiled-coil motif of PHR transcription factors to regulate plant phosphate homeostasis.

Martina K. Ried[1,*,%], Rebekka Wild[1,*,#], Jinsheng Zhu[1], Larissa Broger[1], Robert K. Harmel[2], Ludwig A. Hothorn[3,&], Dorothea Fiedler[2], Michael Hothorn[1,§]

ORCID IDs: MKR: 0000-0003-1582-5016, RW: 0000-0003-2025-7228. JZ: 0000-0002-8131-1876, LB: 0000-0002-1303-9778, RKH: 0000-0003-4413-7730, DF: 0000-0002-0798-946X, MH 0000-0002-3597-5698

[1]Structural Plant Biology Laboratory, Department of Botany and Plant Biology, University of Geneva, 1211 Geneva, Switzerland.

[2]Leibniz-Forschungsinstitut für Molekulare Pharmakologie, 13125 Berlin, Germany & Department of Chemistry, Humboldt-Universität zu Berlin, 12489 Berlin, Germany.

[3]Institute of Biostatistics, Leibniz University, 30419 Hannover, Germany.

[*]contributed equally

[%]Present address: Leibniz Institute of Plant Biochemistry, 06120 Halle, Germany.

[#]Present address: Institut de Biologie Structurale (IBS), 38044 Grenoble, France.

[&]retired

[§]To whom correspondence should be addressed. Email: michael.hothorn@unige.ch

Running title: SPX – transcription factor interaction

Abstract

Phosphorus is an essential nutrient taken up by organisms in the form of inorganic phosphate (Pi). Eukaryotes have evolved sophisticated Pi sensing and signalling cascades, enabling them to maintain cellular Pi concentrations. Pi homeostasis is regulated by inositol pyrophosphate signalling molecules (PP-InsPs), which are sensed by SPX-domain containing proteins. In plants, PP-InsP bound SPX receptors inactivate Myb coiled-coil (MYB-CC) Pi starvation response transcription factors (PHRs) by an unknown mechanism. Here we report that a $InsP_8$ – SPX complex targets the plant-unique CC domain of PHRs. Crystal structures of the CC domain reveal an unusual four-stranded anti-parallel arrangement. Interface mutations in the CC domain yield monomeric PHR1, which is no longer able to bind DNA with high affinity. Mutation of conserved basic residues located at the surface of the CC domain disrupt interaction with the SPX receptor *in vitro* and *in planta*, resulting in constitutive Pi starvation responses. Together, our findings suggest that $InsP_8$ regulates plant Pi homeostasis by controlling the oligomeric state and hence the promoter binding capability of PHRs via their SPX receptors. (173 words)

Introduction

Phosphorus is an essential building block for many cellular components such as nucleic acids and membranes. It is essential for energy transfer and storage and can act as a signalling molecule. Pro- and eukaryotes have evolved intricate systems to acquire phosphorus in the form of inorganic phosphate (Pi), to maintain cytosolic Pi concentrations, and to transport and store Pi as needed. In green algae and plants, transcription factors have been previously identified as master regulators of Pi homeostasis and Pi starvation responses (PSR)[1,2]. Phosphorus starvation response 1 (CrPsr1) from Chlamydomonas and PHOSPHATE STARVATION RESPONSE 1 (AtPHR1) from Arabidopsis were founding members of plant unique MYB-type coiled-coil (MYB-CC) transcription factors[3]. PHR transcription factors were subsequently characterized as regulators of Pi starvation responses in diverse plant species[4–6]. In Arabidopsis there are 15 MYB-CCs with PHR1 and PHL1 controlling the majority of the transcriptional Pi starvation responses[7,8]. Knock-out mutations in *Arabidopsis thaliana PHR1* result in impaired responsiveness of Pi starvation induced (PSI) genes, and perturbed anthocyanin accumulation, carbohydrate metabolism and lipid composition[2,9,10]. Overexpression of *AtPHR1* causes elevated cellular Pi concentrations and impacts the transcript levels of At*PHO2,* which codes for an E2 ubiquitin conjugase involved in PSR, via increased production of its micro RNA miR399d[9,11]. PHR binds to a GNATATNC motif (P1BS), found highly enriched in the promoters of PSI genes and in other *cis*-regulatory motifs, activating gene expression[2,12]. AtPHR1 is not only implicated in Pi homeostasis, but also in sulphate, iron and zinc homeostasis as well as in the adaption to high-light stress[13–16]. Moreover, AtPHR1 shapes the plant root microbiome by negatively regulating plant immunity[17].

AtPHR1 and OsPHR2 have been previously reported physically interact with stand-alone SPX proteins[18–21], additional components of PSR in plants[21–24]. SPX proteins may regulate PHR function by binding to PHRs under Pi sufficient condition, keeping the transcription

62 factor from entering the nucleus[25–27]. Alternatively, binding of SPX proteins to PHRs may
63 reduce the ability of the transcription factors to interact with their promoter core
64 sequences[19,20,25,26,28]. Two mechanisms were put forward regarding the regulation of the SPX –
65 PHR interaction in response to changes in nutrient availability: SPX domains were proposed
66 to act as direct Pi sensors, with the SPX – PHR interaction occurring in the presence of
67 millimolar concentrations of Pi[19,20]. Alternatively, the integrity of the SPX – PHR complex
68 could be regulated by protein degradation. Indeed, SPX degradation via the 26S proteasome is
69 increased under Pi starvation[25,26,29].
70 Fungal, plant and human SPX domains[30] have been independently characterized as cellular
71 receptors for inositol pyrophosphates (PP-InsPs), which bind SPX domains with high affinity
72 and selectivity[31,32]. PP-InsPs consist of a fully phosphorylated *myo*-inositol ring, carrying one
73 or two pyrophosphate groups at the C1 and/or C5 position, respectively[33]. In plants, inositol
74 1,3,4-trisphosphate 5/6-kinase (ITPK) catalyzes the phosphorylation of phytic acid ($InsP_6$) to
75 5PP-$InsP_5$ ($InsP_7$ hereafter)[34]. The diphosphoinositol pentakisphosphate kinases VIH1 and
76 VIH2 then generate 1,5$(PP)_2$-$InsP_4$ ($InsP_8$ hereafter) from $InsP_7$[32,35–37]. Plant diphosphoinositol
77 pentakisphosphate kinases have been genetically characterized to play a role in jasmonate
78 perception and plant defence responses[36] and, importantly, in nutrient sensing in
79 Chlamydomonas[38] and Arabidopsis[32,37]. *vih1 vih2* double mutants lack the PP-InsP messenger
80 $InsP_8$, over accumulate Pi and show constitutive PSI gene expression[32,37]. A *vih1 vih2 phr1*
81 *phl1* quadruple mutant rescues the *vih1 vih2* seedling phenotypes and displays wild type like
82 Pi levels, suggesting that VIH1, VIH2, PP-InsPs and PHRs are part of a common signalling
83 pathway[37]. In line with, the AtSPX1 – AtPHR1 interaction is reduced in *vih1 vih2* mutant
84 plants when compared to wild type[32]. Thus, biochemical and genetic evidence implicates
85 $InsP_8$ in the formation of a SPX – PHR complex[32,37].
86 Cellular $InsP_8$ pools are regulated by nutrient availability at the level of the VIH enzymes
87 themselves. Plant VIH1 and VIH2 and diphosphoinositol pentakisphosphate kinases from

other organisms are bifunctional enzymes, with an N-terminal kinase domain that generates $InsP_8$ from $InsP_7$, and a C-terminal phosphatase domain that hydrolyses $InsP_8$ to $InsP_7$ and $InsP_6$[37,39,40]. The relative enzymatic activities of the two domains are regulated in the context of the full-length enzyme: Under Pi starvation, cellular ATP levels are reduced, leading to a reduction of the VIH kinase activity, and a reduction of $InsP_8$[32,37]. Pi itself acts as an allosteric regulator of the phosphatase activity[37,39]. Thus, under Pi sufficient growth conditions $InsP_8$ accumulates and triggers the formation of a SPX – $InsP_8$ – PHR complex. Under Pi starvation, $InsP_8$ levels drop and the complex dissociates[41].

How the $InsP_8$ bound SPX receptor inactivates PHR function remains to be understood at the mechanistic level. It has been previously reported that AtPHR1 binds P1BS as a dimer[2]. Addition of SPX domains reduces the DNA binding capacity of PHRs as concluded from electophoretic mobility shift assays (EMSA)[19,20,25]. Qi and colleagues reported that AtPHR1 recombinantly expressed as a maltose-binding protein (MBP) fusion protein forms monomers in solution and binds DNA. This process that can be inhibited by preincubating the recombinant transcription factor with AtSPX1 in the presence of high concentrations of $InsP_6$[28]. A recent crystal structure of the AtPHR1 MYB domain in complex with a promoter core fragment supports a dimeric binding mode of MYB-CC transcription factors[42]. Here we investigate the oligomeric state of PHRs, their DNA binding kinetics, and the targeting mechanism of the interacting SPX receptors.

Results

PP-InsPs trigger AtSPX1 - AtPHR1 complex formation in yeast

The interaction of AtSPX1 with AtPHR1 has been previously characterized in yeast-2-hybrid assays[19]. We reproduced the interaction of full-length AtPHR1 and AtSPX1 (Fig. 1a) and verified that all four stand-alone AtSPX proteins (AtSPX1 – 4) interact with a AtPHR1

fragment (AtPHR1$^{226 - 360}$) that contains the MYB domain as well as the CC domain in yeast (Supplementary Fig. 1a). This is in line with previous findings, reporting interaction of SPX domains with larger PHR fragments also containing the MYB and CC domains (AtSPX1 – AtPHR1$^{208-362}$ and OsSPX1/2 – OsPHR2$^{231-426}$)[19,20].

We next tested if the SPX – PHR interactions observed in yeast are mediated by endogenous PP-InsPs. The putative PP-InsP binding surface in AtSPX1 was mapped by homology modeling, using the *Chaetomium thermophilum* GDE1 – $InsP_6$ complex structure (PDB-ID 5IJJ) as template[31]. We replaced putative PP-InsP binding residues from the previously identified Phosphate Binding Cluster (PBC: AtSPX1$^{Y25,\ K29,\ K139}$) and Lysine (K) Surface Cluster (KSC: AtSPX1$^{K136,\ K140,\ K143}$)[31] with alanines (Supplementary Fig. 1b). The resulting AtSPX1^{PBC} and AtSPX1^{KSC} mutant proteins failed to interact with AtPHR1$^{226-360}$ in yeast-2-hybrid assays, while mutation of a conserved lysine residue outside the putative PP-InsP binding site (SC: structural control, AtSPX1^{K81}) to alanine had no effect (Supplementary Fig. 1b). We next deleted the known yeast PP-InsP kinases Vip1, which converts $InsP_6$ to 1PP-$InsP_5$ and 5PP-$InsP_5$ to 1,5(PP)$_2$-$InsP_4$, or Kcs1, which converts $InsP_6$ to 5PP-$InsP_5$ and 1PP-$InsP_5$ to 1,5(PP)$_2$-$InsP_4$[43,44] (Supplementary Fig. 1c,d). We found that deletion of either kinase reduced the interaction between wild type AtSPX1 and AtPHR1$^{226-360}$ (Supplementary Fig. 1c). The interaction between the plant brassinosteroid receptor kinase BRI1 and the inhibitor protein BKI1, known to occur independently of PP-InsPs[45], was not effected in either Δvip1 or Δkcs1 mutants (Supplementary Fig. 1c).

Using quantitative isothermal titration calorimetry (ITC) binding assays, we have previously determined dissociation constants (K_D) for $InsP_6$ and $InsP_7$ binding to a OsSPX4 – OsPHR2 complex to be ~50 and ~7 µM, respectively[31]. A side-by-side comparison of $InsP_7$ and $InsP_8$ binding to OsSPX4 – OsPHR2 by ITC revealed dissociation constants of ~7 and ~3 µM, respectively (Fig. 1b). Taken together, the SPX – PHR interaction is mediated by PP-InsPs, with the *bona fide* Pi signaling molecule $InsP_8$ being the preferred ligand *in vitro*.

AtSPX1 interacts with a unique four-stranded coiled-coil domain in AtPHR1

We next mapped the SPX – PP-InsP binding site in AtPHR1 to a fragment (AtPHR1$^{280-353}$), which comprises the CC domain and a 30 amino-acid spanning N-terminal extension, in yeast-2-hybrid experiments (Fig. 1a). We sought to crystallize an AtSPX1 – PP-InsP – AtPHR1 complex either in the pre- or absence of P1BS fragments. We obtained crystals of a putative AtSPX1 – $InsP_8$ - AtPHR1$^{280-360}$ complex diffracting to 2.4 Å resolution, and solved the structure by molecular replacement, using isolated SPX domain structures as search models[31]. Iterative cycles of model building and crystallographic refinement yielded, to our surprise, a well-refined model of AtPHR1$^{280-360}$ only (see Methods). Analysis with the program PISA revealed the presence of a crystallographic tetramer in which four long α-helices fold into an unusual anti-parallel four-stranded coiled-coil (Fig. 1c). AtPHR1$^{280-360}$ residues 292-356 and 310-357 are visible in the electron density maps from chain A and B, respectively. Residues 292-311 in chain A fold into a protruding loop region that harbors a small α-helix, and appear disordered in chain B (Fig. 1c). The anti-parallel α-helices in AtPHR1 closely align with a root mean square deviation, (r.m.s.d.) of ~ 0.5 Å comparing 45 corresponding C_α atoms. Structural homology searches with the program DALI[46] returned different coiled-coil structures, with a monomer of the tetrameric coiled-coil domain of the yeast transcription factor Ctp1 representing the closest hit (DALI Z-score 5.9, r.m.s.d. is ~1 Å comparing 45 corresponding C_α atoms) (Fig. 1d)[47]. However, no anti-parallel four-stranded coiled-coil domain with structural similarity to AtPHR1 was recovered, with, for example, the Ctp1 dimer-of-dimers domain having a very different configuration (Fig. 1e)[47].

We next assessed the oligomeric state of AtPHR$^{280-360}$ using size-exclusion chromatography coupled to right-angle light scattering (SEC-RALS) and determined an apparent molecular weight of ~37.5 kDa, thus confirming that the isolated AtPHR1 CC forms tetramers in solution (theoretical molecular weight of the monomer is ~9.5 kDa) (Fig. 2a). Two additional

crystal structures of AtPHR1$^{280\text{-}360}$ obtained in different crystal lattices all revealed highly similar tetrameric arrangements (Supplementary Fig. 2, Table 5).

Mutations in the CC domain abolish AtPHR1 oligomerization and DNA binding *in vitro*

It has been recently reported that a AtPHR1$^{208\ -\ 360}$ fragment, which contains both the MYB and the CC domains fused to a maltose binding protein (MBP) tag, forms monomers in solution[48]. In contrast, our AtPHR1$^{280\text{-}360}$ CC fragment is a tetramer (Fig. 2a). We thus purified untagged AtPHR1$^{222\ -\ 358}$ that comprises the CC and the MYB DNA-binding domains, and performed SEC-RALS experiments. We found that AtPHR1$^{222\text{-}358}$ behaves as a dimer in solution (Fig. 2a,b; black traces), in agreement with earlier reports[2]. The observed oligomeric state differences between our AtPHR1$^{280\text{-}360}$ (CC) and AtPHR1$^{222\text{-}358}$ MYB-CC prompted us to investigate the dimer- and tetramerization interfaces in our AtPHR1 structures with the program PISA[49]. We found the dimerization (~1,400 Å^2 buried surface area) and the tetramerization (~1,900 Å^2 buried surface area) interfaces to be mainly formed by hydrophobic interactions (Supplementary Fig. 3a,b). Both interfaces are further stabilized by hydrogen bond interactions and several salt bridges (Supplementary Fig. 3a,b). Importantly, all contributing amino-acids represent sequence fingerprints of the plant unqiue MYB-CC transcription factor subfamily and are highly conserved among different plant species (Supplementary Fig. 3c). We identified residues specifically contributing to the formation of a CC dimer (Olig1: AtPHR1^{L319}, AtPHR1^{I333}, AtPHR1^{L337}, shown in cyan in Fig. 2 and Supplementary Fig. 3) or tetramer (Olig2: AtPHR1^{L317}, AtPHR1^{L327}, AtPHR1^{I341}, shown in dark-orange in Fig. 2 and Supplementary Fig. 3) in our different CC structures (Supplementary Table 5). We replaced these residues by asparagine to generate two triple mutants in AtPHR1$^{222\ -\ 358}$ and AtPHR1$^{280\text{–}360}$, respectively. We found in SEC-RALS assays that both mutant combinations dissolved AtPHR1$^{280\text{–}360}$ tetramers and AtPHR1$^{222\text{–}358}$ dimers into stable monomers, respectively (Fig. 2a,b).

It has been recently reported that the AtPHR1 MYB DNA-binding domain associates with its target DNA as a dimer[42]. We thus studied the capacity of AtPHR1$^{222-358}$ oligmerization mutants to interact with the P1BS in qualitative EMSA and quantitative grating coupled interferometry (GCI) assays. AtPHR1$^{222-358\ Olig1}$ could still interact with the P1BS in EMSAs indistinguishable from wild type (Fig. 2c). However, AtPHR1$^{222-358\ Olig1}$ and AtPHR1$^{222-358\ Olig2}$ bound a biotinylated P1BS immobilized on the GCI chip with ~20-fold reduced affinity when compared to the wild type control (Fig. 2d-f). Together, our experiments suggest that PHR1 MYB-CC exists as a dimer in solution, and that disruption of its plant unique CC domain interface reduces the capacity of the transcription factor to bind its DNA recognition site.

CC surface mutations abolish PHR – SPX interactions but do not interfere with DNA binding *in vitro*

We next sought to identify the binding site for SPX-InsP_8 in the PHR CC domain. In our structures, a conserved set of basic residues maps to the surface of the four CC helices (shown in magenta in Fig. 3a, Supplementary Fig. 3c). A similar set of surface exposed basic residues has been previously found to form the binding site for PP-InsPs in various SPX receptors[31]. Mutation of AtPHR1^{K325}, AtPHR1^{H328}, AtPHR1^{R335}, but not of AtPHR1^{K308}, AtPHR1^{R318}, AtPHR1^{R340} to alanine, disrupted the interaction of AtPHR1 with AtSPX1 in yeast (Fig. 3b). We next simultaneously mutated the residues corresponding to AtPHR1^{K325}, AtPHR1^{H328}, AtPHR1^{R335} to alanine in OsPHR2 (OsPHR2^{KHR}). The mutant transcription factor showed no detectable binding to OsSPX4-InsP_7 in quantitative ITC assays, but maintained the ability to bind the P1BS (Fig. 3c-d). In line with this, mutation of the KHR motif does not alter the oligomeric state of AtPHR1$^{280-360}$ as concluded from SEC-RALS experiments (Fig. 2a, magenta traces). Taken together, three highly conserved basic residues located at the surface of the PHR CC domain are critical for the interaction with the PP-InsP bound SPX receptor (Supplementary Fig. 3c).

Mutation of the AtPHR1 KHR motif impairs AtSPX1 binding and Pi homeostasis *in planta*

We next tested if mutation of the SPX binding site in AtPHR1 can modulate its function in Pi homeostasis in Arabidopsis. We expressed wild-type and point-mutant versions of AtPHR1 carrying an N-terminal FLAG tag under the control of its native promoter in a *phr1-3* loss-of-function mutant[9]. At seedling stage, we found that AtPHR1 single, double and triple point mutations complemented the previously characterized Pi deficiency phenotype of *phr1-3*[2,9]. (Fig. 4a, Supplementary Fig. 4a). After transferring the seedlings to soil, variable growth phenotypes became apparent 21 days after germination (DAG) (Supplementary Fig 4b). From three independent lines per genotype, we selected one line each showing similar *AtPHR1* transcript levels for all experiments shown in Figure 4 (Fig. 4, Supplementary Fig. 5a). Comparing these lines, we found that AtPHR1^{K325A,R335A} double and AtPHR1^{K325A,H328A,R335A} triple mutants, but not the single mutants displayed severe growth phenotypes, with the triple mutant showing the strongest defects (Fig. 4a). We next determined cellular Pi levels in all independent lines and found that i) Pi levels are positively correlated with AtPHR1 expression levels (Supplementary Fig. 5a), that ii) all AtPHR1 mutant proteins tested accumulate Pi to significantly higher levels when compared to wild type and *phr1-3*, and that iii) the AtPHR1^{K325A,H328A,R335A} triple mutant displayed the highest Pi levels (Fig. 4b, Supplementary Fig. 5b-d). In line with this, PSI gene expression is misregulated in AtPHR1^{K325A,R335A} double and AtPHR1^{K325A,H328A,R335A} triple mutants (Fig. 4c). In co-immunoprecipitation assays in *Nicotiana benthamiana* and in Arabidopsis, we found the interaction of AtPHR1^{K325A,H328A,R335A} with AtSPX1 to be reduced when compared to wild-type AtPHR1 (Fig. 4d, Supplementary Fig. 6).

We next studied the genetic interaction between *PHR1* and *VIH1/2*. As previously reported, the severe phenotypes of *vih1-2 vih2-4* seedlings are partially rescued in the *phr1 phl1 vih1-2 vih2-4* quadruple mutant, suggesting that VIH1/2 generated $InsP_8$ regulates the activity of

PHR1 and PHL1 by promoting the binding of SPX receptors[37,32]. We performed the orthogonal genetic experiment, by complementing the *phr1 phl1* mutant with AtPHR1$^{KHR/AAA}$ expressed under the control of the AtPHR1 promoter and carrying a N-terminal eGFP tag (Fig. 4e, see Methods). The complemented lines displayed intermediate growth phenotypes and constitutive PSI gene expression (Fig. 4e,f). Thus, SPX-InsP$_8$ mediated regulation of PHR1 and PHL1 has to be considered one of several PP-InsP regulated processes affected in the *vih1-2 vih2-4* mutant. Together, our *in vivo* experiments reveal that SPX receptors interact with the CC domain of AtPHR1 via the surface exposed Lys325, His328 and Arg335, and that this interaction negatively regulates PHR activity and Pi starvation responses.

Discussion

PHR transcription factors have been early on recognized as central components of the PSR in green algae and in plants, directly regulating the expression of PSI genes[1,2,12]. In Arabidopsis and in rice *spx* mutants of then unknown function also showed altered PSI gene expression[22,24]. This genetic interaction was later substantiated by demonstrating that stand-alone plant SPX proteins can interact with PHR orthologs from Arabidopsis and rice[19,20,25]. The biochemical characterization of SPX domains as cellular receptors for PP-InsPs and the genetic identification of VIH kinases as master regulators of PSR in plants suggested that PP-InsPs, and specifically InsP$_8$ mediates the interaction of SPX proteins with PHRs in response to changing nutrient conditions[31,32,37].

Our quantitative DNA binding assays demonstrate that AtPHR1 MYB-CC binds the P1BS from the *AtSPX1* promoter with high affinity (K_D ~ 0.2 µM), in agreement with previously reported binding constants for different MYB-CC constructs (K_D ~0.01 – 0.1µM)[28,42]. Different oligomeric states have been reported for various PHR MYB-CC constructs[2,28]. Our AtPHR1 MYB-CC construct behaves as a dimer in solution, consistent with the recently reported crystal structure of the AtPHR1 MYB – DNA complex, and with earlier reports[2,42].

We could not assess the oligomeric state of full-length AtPHR1, due to rapid degradation of the recombinant protein. In yeast-2-hybrid assays, we found that AtSPX1-4 all are able to interact with AtPHR1 (Fig. 1a, Supplementary Fig. 1a). We mapped their conserved interaction surface to the plant-unique CC motif of PHRs (Fig. 1a). Crystal structures of this fragment reveal an unusual, four-stranded anti-parallel coiled-coil domain (Fig. 1c). Given the fact, that AtPHR1 MYB-CC forms dimers in solution (Fig. 2b), we cannot exclude the possibility that the CC tetramers represent crystal packing artifacts. However, we did observe identical CC tetramers in three independent crystal lattices (Supplementary Fig. 2) and in solution (Fig. 2a). The residues contributing to the dimer and to the tetramer interfaces are highly conserved among all plant MYB-CC transcription factors (Supplementary Fig. 3). Mutation of either interface blocks AtPHR1 oligomerization *in vitro* (Fig. 2a,b), and reduces DNA binding (Fig 2d-f). An attractive hypothesis would thus be that AtPHR1 binds its target promoter as a dimer, but can potentially form hetero-tetramers with other MYB-CC type transcription factors sharing the conserved, plant-unique CC structure and sequence (Supplementary Fig. 3). Notably, PHR1 PHL1 heteromers have been previously described[12].

We found that SPX – PHR complex formation is mediated by endogenous PP-InsPs in yeast cells, as deletion of the yeast PP-InsP kinases Vip1 and Kcs1 abolished the interaction, and mutation of the PP-InsP binding surface in AtSPX1 interfered with AtPHR1 binding (Supplementary Fig. 1b,c). In line with this, SPX – PHR complexes are found dissociated in *vih1 vih2* mutant plants[32]. It is of note that the observed differences in binding affinity for $InsP_7$ and $InsP_8$ to SPX – PHR *in vitro* (Fig. 1b)[32] cannot fully rationalize the apparent preference for $InsP_8$ *in vivo*[32,37]. We identified the binding surface for SPX-$InsP_8$ by locating a set of highly conserved basic residues exposed at the surface of the CC domain (Fig. 3a, Supplementary Fig. 3). Mutation of this KHR motif did not strongly impact the ability of isolated OsPHR2 to bind *pOsIPS1 in vitro* (Fig. 3d), but disrupted the interaction of AtPHR1

with AtSPX1 in yeast (Fig. 3b). The corresponding mutations in OsPHR2 had a similar effect on the interaction with OsSPX4 in quantitative ITC assays (Fig. 3c). Expression of AtPHR1$^{KHR/AAA}$ in the *phr1-3* mutant resulted in Pi hyperaccumlation phenotypes and constitutive PSI gene expression in Arabidopsis (Fig. 4a-c). The intermediate growth phenotypes of *vih1 vih2 phr1 phl1* mutants complemented with AtPHR1$^{KHR/AAA}$ clearly suggests that PP-InsPs do not only regulate the activity of PHR1 and PHL1 in plants, but likely the function of other (SPX domain-containing) proteins[31] (Fig. 4e). Notably, binding of AtPHR1^{KHR} to AtSPX1 was reduced in co-immunoprecipitation assays when compared to wild type AtSPX1 (Fig. 4d, Supplementary Fig. 6). Thus, our and previous finding suggest that $InsP_8$ can act as a molecular glue, promoting the association of SPX receptors and PHR transcription factors. The interaction surface is likely formed by the previously characterized SPX basic surface patch[31], and by the newly identified basic surface area in PHR CC, harboring the conserved KHR motif (Fig. 3a).

It is of note that addition of AtSPX1 to AtPHR1 has been previously demonstrated to reduce AtPHR1's ability to bind to P1BS in the presence of $InsP_6$[28]. We could not quantify these interactions in ITC or GCI binding assays, as PHR CC formation is much preferred over SPX-$InsP_8$ binding at the protein concentrations required in these assays. We speculate that $InsP_8$ bound SPX proteins can bind to the basic residues we identified in the PHR CC domain to control the oligomeric state and hence the promoter binding capacity of PHRs. As these residues are conserved among all plant MYB-CC proteins this may suggest that transcription factors outside the PHR sub-family may be regulated by SPX domains and PP-InsPs, possibly rationalizing the severe phenotypes of *vih1 vih2* mutant plants (Fig. 4e, Supplementary Fig. 3). The recent findings that VIH kinases and PHRs act together in plant PSR and that SPX-PHR complexes are dissociated in *vih1 vih2* mutants further suggest that $InsP_8$ is the *bona fide* signaling molecule promoting the association between SPX domains and MYB-CCs[32,37].

Repressive SPX – PHR complexes consequently form only under Pi sufficient conditions, where $InsP_8$ levels are high[32,37]. Under Pi starvation, when $InsP_8$ levels are reduced, SPX - PHR complexes dissociate, enabling the transcription factors to acquire the oligomeric state required for high affinity promoter binding. The physiological and mechanistic investigation of this central process may, in the long term, contribute to the development of Pi starvation resilient crops. This could in turn sustain the use of the essential and non-renewable resource rock phosphate, which is currently consumed at an alarming scale.

Methods

Molecular cloning, constructs and primers

For a detailed description of the cloning strategies, constructs and primers used in this study, please refer to Supplementary Table 2 and Table 3a -c.

Generation of stable transgenic *A. thaliana* lines

All stable transgenic *A. thaliana* lines are listed in Supplementary Table 1. Constructs were introduced into *Agrobacterium tumefaciens* strain pGV2260 and *A. thaliana* plants were transformed via floral dipping[50]. Transformants were identified by mCherry fluorescence with a Zeiss Axio Zoom.V16 stereo microscope (mRFP filter) and a HXP200C illuminator. Homozygous T3 lines have been identified for complementation lines expressing FLAG-AtPHR1, FLAG-AtPHR1^{K325A}, FLAG-AtPHR1^{H328A}, FLAG-AtPHR1^{R335A} under the control of the native *AtPHR1* promoter. For complementation lines expressing FLAG-AtPHR1$^{K325A\ R335A}$ and FLAG-AtPHR1$^{K325A\ H328A\ R335A}$ under the control of the native *AtPHR1* promoter, T2 lines were used throughout, and homozygous and heterozygous transformants were selected for all experiments by mCherry fluorescence as described above. T3 homozygous lines expressing eGFP-PHR1 under the control of the *AtPHR1* promoter were identified by their Hygromycin resistance. PHR1 was amplified from Arabidopsis cDNA and introduced

into pH7m34GW binary vector. Point mutations were introduced by site-directed mutagenesis (primers are listed in Supplementary Table 3f).

Yeast-two hybrid experiments

(Screen) AtSPX1$^{1-252}$ was used as a bait and screened against an *A. thaliana* seedling cDNA library by Hybrigenics Services. AtSPX1$^{1-252}$ was cloned into the pB29 vector providing a C-terminal LexA-DNA binding domain (BD) and transformed into yeast strain L40αGal4 (MATa). Prey genes were cloned into the pP6 vector providing a N-terminal Gal4 activation domain (AD) and transformed into yeast strain YHGX13 (MATα). After mating haploid bait and prey strains, positive interactions were detected by growth on histidine deficient medium.

(Yeast strains and media) For all experiments, either the diploid TATA strain (Hybrigenics Services) or the haploid L40 strain was used (Supplementary Table 2). Cells were routinely maintained on YPAD plates (20 g/L glucose, 20 g/L bacto-peptone, 10 g/L yeast extract, 0.04 g/L adenine hemisulfate, 20 g/L agar). Experiments were performed on synthetic dropout (SD) plates (6.7 g/L yeast nitrogen base with adenine hemisulfate and without leucine, tryptophan and histidine, 20 g/L glucose, 20 g/L agar) supplemented with 0.076 g/L histidine or 10 mM 3-amino,1,2,4-triazole (3-AT).

(Yeast transformation) One yeast colony was resuspended in 500 µL sterile H_2O, plated on YPAD plates and grown for two days until the whole plate was covered with yeast. Yeast cells were then resuspended in 50 mL YPAD liquid medium and the OD_{600nm} was determined ($2*10^6$ cells/mL were used for one transformations). Cells were centrifuged at 3,000 xg and 4°C for 5 min, resuspended in 25 mL TE buffer, centrifuged again at 3,000 xg and 4°C for 5 min, resuspended in 2 mL LiAc/TE buffer, centrifuged at 16,000 xg and RT for 15 s, and finally resuspended in 50µL/transformation LiAc/TE buffer. The transformation mix (0.5 µg bait plasmid, 0.5 µg prey plasmid, 10 µL ssDNA (10 mg/mL), 50 µL yeast cells, 345 µL 40% (w/v) PEG3350 in LiAC/TE) was prepared and incubated at 30°C for 45 minutes, followed by incubation at 42°C for 30 min. Finally, yeast cells were centrifuged at 6,500 xg and RT for 15

s, resuspended in TE buffer, plated on SD plates lacking leucine and tryptophan and incubated at 30°C for 3 days.

(Yeast spotting dilution assay) Positive transformants were selected on SD plates without tryptophan and leucine, and incubated at 30°C for three days. Cells were counted, washed in sterile water and spotted in 5 times dilution (5000, 1000, 200, 40, 8 cells) on SD plates without either tryptophan and leucine, or tryptophan, leucine and histidine supplemented with 10 mM 3-AT. Plates were incubated at 30°C for 3 days.

Protein expression and purification

(AtPHR1, OsPHR2 and OsSPX4) AtPHR1$^{280\text{-}360\ wt/KHR/Olig1/Olig2}$ and AtPHR1$^{222\text{-}358\ wt/Olig1/Olig2}$ were cloned into the pMH-HT protein expression vector, providing a N-terminal 6xHis affinity tag with a tobacco etch virus (TEV) protease recognition site. OsPHR2$^{1\text{-}426\ wt/KHR}$ was cloned into the pMH-HSgb1T protein expression vector, providing a N-terminal 8xHis-Strep-gb1 affinity tag with a TEV cleavage site. OsSPX2$^{1\text{-}321}$ was cloned into the pMH-HSsumo protein expression vector, providing a N-terminal 8xHis-Strep-Sumo affinity tag. All constructs were transformed into *E. coli* BL21 (DE3) RIL cells. For recombinant protein expression, cells were grown at 37ºC in terrific broth (TB) medium to an OD_{600nm} of 0.6. After reducing the temperature to 18ºC, protein expression was induced with 0.3 mM isopropyl β-D-galactoside (IPTG) for 16 h. Cells were centrifuged at 2,200 rpm and 4°C for 1 h, resuspended in lysis buffer (50 mM Tris-HCl pH 7.8, 500 mM NaCl, 0.1% (v/v) IGEPAL, 1mM MgCl, 2mM β-mercaptoethanol), snap-frozen in liquid nitrogen and stored at -80°C. For protein preparation, cells were thawed, supplemented with cOmplete^{TM} EDTA-free protease inhibitor cocktail (Roch), DNaseI, and lysozyme, and disrupted using a sonicator. Cell lysates were centrifuged at 7,000 xg and 4°C for 1 h, sterile filtered, supplemented with 20 mM imidazole and loaded onto a 5 mL HisTrap HP Ni^{2+} affinity column (GE Healthcare). After washing with several column volumes (CV) of lysis buffer supplemented with 20 mM imidazole, high salt buffer (50 mM Tris-HCl pH 7.8, 1M NaCl, 2 mM β-mercaptoethanol),

and high phosphate buffer (200 mM K_2HPO_4/KH_2PO_4 pH 7.8, 2 mM β-mercaptoethanol), proteins were eluted in a gradient from 20 to 500 mM imidazole in lysis buffer. The purified proteins were cleaved by TEV or Sumo protease overnight at 4°C (1:100 ratio) and dialyzed against lysis buffer for $PHR1^{222\text{-}358\ wt/Olig1/Olig2}$ and $PHR1^{280\text{-}360\ wt/KHR/Olig1/Olig2}$ fragments, against modified lysis buffer (25 mM Tris-HCl pH 7.8, 300 mM NaCl, 0.1% (v/v) IGEPAL, 1mM MgCl, 2mM β-mercaptoethanol) for $OsPHR2^{1\text{-}426\ wt/KHR}$, and against modified anion exchange buffer (20 mM Tris-HCl pH 6.5, 500 mM NaCl) for $OsSPX4^{1\text{-}321}$. $PHR1^{280\text{-}360\ wt/KHR/Olig1/Olig2}$ and $OsPHR2^{1\text{-}426\ wt/KHR}$ were subjected to a second Ni^{2+} affinity purification in either lysis buffer or modified lysis buffer, respectively, and the flow-throughs were collected and concentrated. $PHR1^{222\text{-}358\ wt/Olig1/Olig2}$ were subjected to cation exchange (50 mM Hepes pH 7.5, 50 – 1000 mM NaCl), and $OsSPX4^{1\text{-}321}$ was subjected to anion exchange (20 mM Tris-HCl, 50 – 1000 mM NaCl). Fractions corresponding to the respective proteins were pooled and concentrated. All proteins were loaded onto a HiLoad Superdex 75pg HR26/60 column (GE healthcare), pre-equilibrated in gel filtration buffer A (20 mM Tris/HCl pH 7.5, 300 mM NaCl, 0.5 mM TCEP) for $PHR1^{222\text{-}358\ wt/Olig1/Olig2}$, or in gel filtration buffer B (20 mM Tris/HCl pH 7, 200 mM NaCl, 0.5 mM TCEP) for the remaining proteins. Fractions containing the respective proteins were pooled and concentrated. Purified and concentrated protein was immediately used for further experiments or snap-frozen in liquid nitrogen and stored at -80ºC.

(AtPHR1$^{280\text{-}360}$ used for crystallization) The AtPHR1$^{280\text{-}360}$ fragment was cloned into the pMH-HS-Sumo protein expression vector, providing a N-terminal 8xHis-StrepII tandem affinity tag and a Sumo fusion protein. The construct was transformed into *E. coli* BL21 (DE3) RIL cells. For recombinant protein expression, cells were grown at 37ºC in terrific broth (TB) medium to an oD_{600nm} of 0.6. After reducing the temperature to 16ºC, protein expression was induced with 0.3 mM isopropyl β-D-galactoside (IPTG) for 16 h. Cells were centrifuged for 20 min at 4,000 g and 4ºC, then the cell pellet was washed with PBS, snap-

frozen in liquid nitrogen and stored at -80ºC. For protein complex purification, the cell pellet was thawed and mixed with twice the amount of cells expressing a His-Strep-MBP-AtSPX1$^{1-251}$ fusion protein, which provides a N-terminal, TEV-cleavable maltose binding protein (MBP). Lysis buffer (200 mM KP_i pH 7.8, 2 β-ME) supplemented with 0.1% (v/v) IGEPAL, 1 mM $MgCl_2$, 10 mM imidazole, 500 units TurboNuclease (BioVision), 2 tablets Protease Inhibitor Cocktail (Roche) was added and cells were disrupted using an EmulsiFlex-C3 (Avestin). Cell lysates were centrifuged at 7,000 g and 4ºC for 1 h. The cleared supernatant was sterile filtered and loaded onto a 5 mL HisTrap HP Ni^{2+} affinity column (GE Healthcare). After washing with several column volumes of lysis buffer, the protein was eluted with 250 mM imidazole in lysis buffer. The purified His-Strep-Sumo-AtPHR1/His-Strep-MBP-AtSPX1 fusion proteins were cleaved by TEV and Sumo protease treatment overnight at 4ºC while dialyzing in a buffer containing 200 mM KP_i pH 7.8, 100 mM NaCl, 2 β-ME. 10 mM imidazole were added to the cleaved protein sample and a second Ni^{2+} affinity step was performed in order to remove the cleaved-off His-Strep-Sumo/MBP fusion tags as well as the 6xHis-tagged Sumo and TEV proteases. The flow-through was concentrated and loaded onto a HiLoad Superdex 75pg HR16/60 column (GE healthcare), pre-equilibrated in gel filtration buffer (20 mM Tris/HCl pH 7.8, 250 mM NaCl, 2.5 mM $InsP_6$, 0.5 mM TCEP). Fractions containing both, the AtSPX1$^{1-251}$ and AtPHR1$^{280-360}$ proteins, were pooled and concentrated. A second size exclusion chromatography step was performed using a HiLoad Superdex 200pg HR26/60 column (GE healthcare) and the same gel filtration buffer as above. Purified and concentrated protein was immediately used for further experiments or snap-frozen in liquid nitrogen and stored at -80ºC.

Isothermal titration calorimetry (ITC)

All ITC experiments were performed at 25°C using a MicroCal PEAQ-ITC system (Malvern Panalytical) equipped with a 200 µl sample cell and a 40 µl injection syringe. 5PP-$InsP_5$ ($InsP_7$) and 1,5$(PP)_2$-$InsP_4$ ($InsP_8$) were produced as described[51]. All proteins were dialysed

against ITC buffer (20 mM HEPES pH 7.0, 200 mM NaCl) and PP-InsP ligands were diluted in ITC buffer prior to all measurements. A typical titration consisted of 15 injections, the protein concentrations in the syringe and in the cell are provided in the respective figure legend. Data were analyzed using the MicroCal PEAQ-ITC analysis software (v1.21).

Crystallization and data collection

Two hexagonal crystal forms developed in sitting drops consisting of 0.2 µL protein at a concentration of 12 mg/mL and 0.2 µL reservoir solution (0.1 M phosphate citrate pH 4.2, 0.2 M NaCl, 20% (w/v) PEG 8000). Crystals were cryo-protected by adding reservoir solution containing 10% (v/v) ethylene glycol directly to the drop and subsequently snap-frozen in liquid nitrogen. A third, tetragonal crystal form developed in 0.1 M Bis-Tri pH 6.5, 0.1 M NaCl, 1.5 M $(NH_4)_2SO_4$. Crystals were cryo-protected by serial transfer into reservoir solution supplemented with 15% (v/v) glycerol and snap-frozen in liquid nitrogen. Crystal forms 1, 2 and 3 diffracted to ~2.4, ~2.5 Å and ~1.9 Å resolution, respectively. Data were collected at beam-line PXIII of the Swiss Light Source (SLS), Villigen, Switzerland. Data processing and scaling was done in XDS[52].

Crystallographic structure solution and refinement

The AtPHR1$^{280\text{-}360}$ structure was solved by molecular replacement using the previously described SPX^{CtGde1} (PDB-ID:5IJJ) core helices as search model in calculations with the program PHASER[53]. The structure was completed in iterative cycles of manual model building in COOT[54] and restrained refinement in phenix.refine[55] or Refmac5[56]. Residues 280-294 and residues 278-280 appear disordered in the final model. Quality of the structural model was assessed by using MolProbity[57], refinement statistics are shown in Supplementary Table 5. Structure visualization was done with PyMOL (Molecular Graphics System, Version 1.7, Schrödinger, LLC) and ChimeraX[58]. The structure of AtSPX1 was modeled using the program SWISS-MODEL[59] and the SPX^{HsXPR1} domain structure of the human phosphate

exporter as template (PDB-ID:5IJH, GMQE score ~ 0.49, QMEAN4 score ~ -2.27, 29.5% sequence identity[60]). Conserved PP-InsP binding residues in AtSPX1 were determined by aligning sequences with previously described SPX domains[31] using the program T-coffee[61].

Right angle light scattering (RALS)

The oligomeric state of AtPHR1 variants was analyzed by size-exclusion chromatography paired with a refractive-index detector using an OMNISEC RESOLVE/REVEAL combined system (Malvern). Instrument calibration was performed with a BSA standard (Thermo Scientific Albumin Standard). Samples of 50 µL containing 2 – 10 mg/mL AtPHR1 (wild type AtPHR1$^{280\text{-}360}$, AtPHR1$^{280\text{-}360\ Olig1}$, AtPHR1$^{280\text{-}360\ Olig2}$, AtPHR1$^{280\text{-}360\ KHR}$, wild type AtPHR1$^{222\text{-}358}$, AtPHR1$^{222\text{-}358\ Olig1}$, AtPHR1$^{222\text{-}358\ Olig2}$) in OMNISEC buffer (20 mM Hepes pH 7.5, 150 mM NaCl) were separated on a Superdex 200 increase 10/300 GL column (GE Healthcare) at a column temperature of 25°C and a flow rate of 0.7 ml min^{-1}. Data were analyzed using the OMNISEC software (v10.41).

DNA oligonucleotide annealing

DNA oligonucleotides were dissolved in annealing buffer (10 mM HEPES-NaOH pH 8.0, 50 mM NaCl, 0.1 mM EDTA). Equal volumes of the equimolar DNA oligonucleotides were mixed and incubated in a heat block for 5 min at 95 °C. Subsequently, DNA oligonucleotides were cooled down to room temperature for 90 min. Double-stranded DNA oligonucleotides were aliquoted and stored at -20°C.

Electrophoretic mobility shift assay (EMSA)

5 % Mini-PROTEAN TBE precast gels (Bio-Rad) have been pre-electrophoresed in 0.5x TBE buffer for 60 minutes at 70 V. Reactions mixes have been prepared following the Odyssey® Infrared EMSA kit manual (LI-COR) without the use of optional components, including 50 nM of IRDye800 end-labeled oligos (refer to Supplementary Table 4a; Metabion), and a 1:5 dilution series of wild type AtPHR1$^{222\text{-}358}$ or AtPHR1$^{222\text{-}358\ Olig1}$ (1.2 µg to 76.8 pg). Reaction

mixes have been incubated for 30 minutes at room temperature in the dark, and 2 µL of 10x Orange Loading Dye (LI-COR) have been added to each sample prior to loading on a 5% TBE gel. Gels have been electrophoresed until orange dye migrated to the bottom of the gel (~ 1 h) at 70 V in the dark. Gels have been scanned with the 800 nm channel of an Odyssey imaging system (LI-COR).

Grating coupled interferometry (GCI)

All GCI experiments were performed at 4°C using a Creoptix WAVE system (Creoptix sensors) with 4PCP WAVE chips (Creoptix sensors). Chips were conditioned with borate buffer (100 mM sodium borate pH 9.0, 1 M NaCl) and subsequently neutravidin was immobilized on the chip surface via standard amine-coupling: activation (1:1 mix of 400 mM *N*-(3-dimethylaminopropyl)-*N'*-ethylcarbodiimide hydrochloride, and 100 mM *N*-hydroxysuccinimide); immobilization (30 µg ml^{-1} of neutravidin in 10 mM sodium acetate, pH 5.0); passivation (5% BSA in 10 mM sodium acetate, pH 5.0); quenching (1 M ethanolamine, pH 8.0). Biotinylated oligos (Supplementary Table 4b; Metabion) were captured on the chip. Analytes were injected in a 1:2 dilution series starting from 4 µM ($AtPHR1^{222-358}$), 20 µM ($AtPHR1^{223-358\ Olig1}$, $AtPHR1^{223-358\ Olig2}$), or 10 µM (OsPHR2, $OsPHR2^{KHR}$) in GCI buffer (for OsPHR2: 20 mM HEPES pH 7.9, 200 mM NaCl; for AtPHR1: 20 mM HEPES pH 7.5, 300 mM NaCl). Blank injections every 4^{th} cycle were used for double referencing and a dimethylsulfoxide (DMSO) calibration curve (0%, 0.5%, 1%, 1.5%, 2%) for bulk correction. Data were corrected and analysed using the Creoptix WAVE control software (corrections applied: X and Y offset; DMSO calibration; double referencing; refractive index correction), and a one-to-one binding model was used to fit all experiments.

Plant material, seed sterilization and plant growth conditions

All *A. thaliana* plants used in this study were of the Columbia (Col-0) ecotype. Seeds of the T-DNA insertion lines *phr1-3* (SALK_067629) and phl1 (SAIL_731_B09) were obtained from the European Arabidopsis Stock Center. Homozygous *phr1-3* and *phl1* lines were

identified by PCR using T-DNA left and right border primers paired with gene-specific sense and antisense primers (Supplementary Table 3d). The *phr1 phl1* double mutant was kindly provided by Yves Poirier (University of Lausanne, Switzerland), *vih1-2 vih2-4* double and *phr1 phl1 vih1-2 vih2-4* quadruple mutants have been reported previously[37]. Seeds were surface sterilized by incubation in 70% (v/v) CH_3-CH_2-OH for 10 minutes, followed by incubation in 0.5% (v/v) sodium hypochlorite for 10 minutes, and subsequently washed four times in sterile H_2O. Seeds were placed on full half-strength Murashige-Skoog plates[63] containing 1 (w/v) % sucrose and 0.8 (w/v) % agar ($^{1/2}$MS plates), and stratified for 2 to 3 d at 4°C in the dark prior to transfer into a growth cabinet. Plants were grown on vertical $^{1/2}$MS plates at 22°C under long day conditions (16 h light – 8 h dark) for 8 to 11 d.

Western blot

Proteins were transferred to nitrocellulose membrane (GE Healthcare, Amersham™ Highbond™-ECL) via wet western blotting at 4°C and 30 V overnight. Membranes were blocked in TBS-Tween (0.1%) - Milk (5%) for one hour at room temperature. For mCherry detection, membranes were incubated overnight with an anti-mCherry antibody (ab167453, dilution 1:2000; Abcam) followed by one hour incubation with an anti-rabbit-HRP antibody (dilution 1:10000, Calbiochem). For GFP detection, membranes were incubated overnight with an anti-GFP-HRP antibody (130-091-833, dilution 1:1000, Miltenyi Biotec). For FLAG detection, membranes were incubated overnight with an anti-FLAG-HRP antibody (A8692, dilution 1:1000, Sigma). Antibodies were diluted in TBS-Tween (0.05%) - Milk (2.5%). Membranes were detected with SuperSignal™ West Femto Maximum Sensitivity Substrate (34095, Thermo Scientific™) and subsequently stained with Ponceau stain (0.1% (w/v) Ponceau S in 5% (v/v) acetic acid).

Determination of cellular Pi concentrations

To determine cellular Pi concentration at seedling stage, plants were transferred from $^{1/2}$MS plates to -Pi $^{1/2}$MS plates containing 1 (w/v) % sucrose and 0.8 (w/v) % agarose supplemented with either 0 mM, 1 mM, or 10 mM Pi (KH_2PO_4/K_2HPO_4; pH 5.7) at 7 DAG, and grown at 22 °C under long day conditions. At 14 DAG, seedlings were weighted and harvested into 1.5 mL tubes containing 500 µL nanopure H_2O. Samples were frozen at -80°C overnight, thawed at 80°C for ten minutes, refrozen at -80°C, incubated at 80°C and 1,400 rpm for one hour and briefly centrifuged to sediment plant tissue. Pi content was measured by the colorimetric molybdate assay[64].

RNA analyses

At 14 DAG, 50 - 150 mg seedlings were harvested in 2 ml Eppendorf tubes containing two metal beads each, shock-frozen in liquid nitrogen and ground in a tissue lyzer (MM400, Retsch). RNA extraction was performed using the ReliaPrep RNA Tissue Miniprep System (Promega) including in column DNase I treatment to remove genomic DNA. First strand cDNA synthesis was performed from 1 µg – 2.5 µg of total RNA using Superscript II RT (Invitrogen) with oligo(dT) primers. qRT-PCR was performed in 10 µL reactions containing 1x SYBR-Green fluorescent stain (Applied Biosystems) and measured using a 7900HT Fast Real Time PCR-System (Applied Biosystems). qRT-PCR programme: 2'-95°C; 40 x (30''-95°C; 30''-60°C; 20''-72°C); melting curve 95°C – 60°C – 95°C. A primer list can be found in Supplementary Table 3e. Expression levels of target genes were normalized against the housekeeping gene *Actin2*. For every genotype, three biological replicates were analyzed in technical triplicates.

Transient transformation of *Nicotiana benthamiana*

For each construct, 4 ml of *A. tumefaciens* strain pGV2260 suspension culture were grown overnight at 28°C. Cells were collected by centrifugation at 700 xg for 15 mins and resuspended in transformation buffer (10 mM $MgCl_2$, 10 mM MES pH 5.6, 150 µM

571 acetosyringone). Cell density was measured and set to a final OD_{600} of 0.5 for SPX1 and
572 PHR1, and to 0.1 for the silencing suppressor P19. Suspension cultures were incubated for
573 two hours in the dark at room temperature and subsequently mixed at a volume ratio of 1:1:1
574 (SPX1:PHR1:P19). *N. benthamiana* leaves were infiltrated using a 0.5-ml syringe and 3 leaf
575 disks (d = 1 cm) per sample were harvested after 3 d, snap-frozen in liquid nitrogen, and
576 stored at – 80°C.

577 **Co-immunoprecipitation**

578 For co-immunoprecipitation experiments with proteins transiently expressed in *N.*
579 *benthamiana*, samples were ground in liquid nitrogen with plastic mortars and proteins were
580 extracted with 600 µL of homogenisation buffer (50 mM Tris-HCl pH 7.5, 150 mM NaCl,
581 0.25% Triton X-100, 5% (v/v) glycerol, 1 mM PMSF, cOmplete™ EDTA-free protease
582 inhibitor cocktail (Roche). Samples were incubated at 4°C for 10 min with gently rotation and
583 subsequently centrifuged at 16,000 xg and 4°C for 15 min. Supernatants were transferred to
584 fresh tubes and further centrifuged at 16,000 xg and 4°C for 15 min. Supernatants were
585 transferred to fresh tubes, while 50 µL of each supernatant were taken and mixed with 10 µL
586 6x SDS sample buffer (input), the remaining supernatants were mixed with 50 µL magnetic
587 µMACS anti-GFP beads (Miltenyi Biotec) and incubated at 4°C for 2 h with gently rotation.
588 MACS columns (Miltenyi Biotec) were used with a µMACS Separator (Milteyi Biotec).
589 MACS columns were washed with 200 µL of homogenisation buffer and samples were
590 loaded. Columns were washed either four times with 200 µL of homogenisation buffer and
591 once with wash buffer 2 (Miltenyi Biotec), or three times with 200 µL of homogenisation
592 buffer, three times with wash buffer 1 (Miltenyi Biotec) and once with wash buffer 2.
593 Columns were incubated with 20 µL preheated elution buffer (Miltenyi Biotec) for 5 min at
594 room temperature. 50 µL of elution buffer were added and eluates were recovered. Inputs and
595 eluates were boiled for 5 min at 95°C prior and separated on 9 % SDS-PAGE gels. Co-

596 immunoprecipitation experiments for proteins stably or natively expressed in *A. thaliana*,
597 were performed as previously described[65].

598 **Statistics**

599 Simultaneous inference was used throughout to limit the false positive decision rate in these
600 randomized one- or two-way layouts. Designs with technical replicates were analysed using a
601 mixed effect model. Normal distributed variance homogeneous errors were assumed when
602 appropriate, otherwise a modified variance estimator allowing group-specific variances was
603 used[66]. Multiple comparisons of several genotypes vs. wild type (Col-0) shown in Fig. 4b, and
604 Supplementary Fig. 5a-d were performed as described[67] (*, $p < 0.5$; **, $p < 0.05$).

605

606 **Data availability**

607 Data supporting the findings of this manuscript are available from the corresponding authors
608 upon reasonable request. A reporting summary for this article is available as a Supplementary
609 Information file. The source data underlying the qPCR and Pi level measurements are
610 provided as Source Data files. Coordinates and structure factors have been deposited in the
611 Protein Data Bank (PDB) with accession codes 6TO5 (form1,
612 https://doi.org/10.2210/pdb6TO5/pdb), 6TO9 (form2, https://doi.org/10.2210/pdb6TO9/pdb)
613 and 6TOC (form 3, https://doi.org/10.2210/pdb6TOC/pdb). The associated X-ray diffraction
614 images and data processing files have been deposited at http://zenodo.org with DOIs 10.5281/
615 zenodo.3570698 (form1), 10.5281/zenodo.3570977 (form 2) and 10.5281/zenodo.3571040
616 (form 3).

617

618 **References**

619 1. Wykoff, D. D., Grossman, A. R., Weeks, D. P., Usuda, H. & Shimogawara, K. Psr1, a
620 nuclear localized protein that regulates phosphorus metabolism in Chlamydomonas. *Proc.*
621 *Natl. Acad. Sci. U. S. A.* **96**, 15336–15341 (1999).
622 2. Rubio, V. *et al.* A conserved MYB transcription factor involved in phosphate starvation
623 signaling both in vascular plants and in unicellular algae. *Genes Dev.* (2001) doi:10.1101/
624 gad.204401.

3. Riechmann, J. L. *et al.* Arabidopsis transcription factors: genome-wide comparative analysis among eukaryotes. *Science* **290**, 2105–2110 (2000).

4. Zhou, J. *et al.* OsPHR2 Is Involved in Phosphate-Starvation Signaling and Excessive Phosphate Accumulation in Shoots of Plants. *Plant Physiol.* **146**, 1673 (2008).

5. Ren, F. *et al.* Brassica napus PHR1 Gene Encoding a MYB-Like Protein Functions in Response to Phosphate Starvation. *PLOS ONE* **7**, e44005 (2012).

6. Wang, J. *et al.* A phosphate starvation response regulator Ta-PHR1 is involved in phosphate signalling and increases grain yield in wheat. *Ann. Bot.* **111**, 1139–1153 (2013).

7. Bustos, R. *et al.* A central regulatory system largely controls transcriptional activation and repression responses to phosphate starvation in arabidopsis. *PLoS Genet.* (2010) doi:10.1371/journal.pgen.1001102.

8. Sun, L., Song, L., Zhang, Y., Zheng, Z. & Liu, D. Arabidopsis PHL2 and PHR1 Act Redundantly as the Key Components of the Central Regulatory System Controlling Transcriptional Responses to Phosphate Starvation. *Plant Physiol.* **170**, 499–514 (2016).

9. Nilsson, L., Müller, R. & Nielsen, T. H. Increased expression of the MYB-related transcription factor, PHR1, leads to enhanced phosphate uptake in Arabidopsis thaliana. *Plant Cell Environ.* (2007) doi:10.1111/j.1365-3040.2007.01734.x.

10. Pant, B. D. *et al.* The transcription factor PHR1 regulates lipid remodeling and triacylglycerol accumulation in Arabidopsis thaliana during phosphorus starvation. *J. Exp. Bot.* (2015) doi:10.1093/jxb/eru535.

11. Bari, R., Pant, B. D., Stitt, M. & Scheible, W. R. PHO2, microRNA399, and PHR1 define a phosphate-signaling pathway in plants. *Plant Physiol.* (2006) doi:10.1104/pp.106.079707.

12. Bustos, R. *et al.* A central regulatory system largely controls transcriptional activation and repression responses to phosphate starvation in arabidopsis. *PLoS Genet.* (2010) doi:10.1371/journal.pgen.1001102.

652 13. Rouached, H., Secco, D., Arpat, B. & Poirier, Y. The transcription factor PHR1 plays a
653 key role in the regulation of sulfate shoot-to-root flux upon phosphate starvation in
654 Arabidopsis. *BMC Plant Biol.* (2011) doi:10.1186/1471-2229-11-19.
655 14. Nilsson, L., Lundmark, M., Jensen, P. E. & Nielsen, T. H. The Arabidopsis transcription
656 factor PHR1 is essential for adaptation to high light and retaining functional
657 photosynthesis during phosphate starvation. *Physiol. Plant.* (2012) doi:10.1111/j.1399-
658 3054.2011.01520.x.
659 15. Bournier, M. *et al.* Arabidopsis ferritin 1 (AtFer1) gene regulation by the phosphate
660 starvation response 1 (AtPHR1) transcription factor reveals a direct molecular link
661 between iron and phosphate homeostasis. *J. Biol. Chem.* (2013)
662 doi:10.1074/jbc.M113.482281.
663 16. Khan, G. A. *et al.* Coordination between zinc and phosphate homeostasis involves the
664 transcription factor PHR1, the phosphate exporter PHO1, and its homologue PHO1;H3 in
665 Arabidopsis. *J. Exp. Bot.* **65**, 871–884 (2014).
666 17. Castrillo, G. *et al.* Root microbiota drive direct integration of phosphate stress and
667 immunity. *Nature* **543**, 513–518 (2017).
668 18. Liu, F. *et al.* OsSPX1 suppresses the function of OsPHR2 in the regulation of expression
669 of OsPT2 and phosphate homeostasis in shoots of rice. *Plant J.* **62**, 508–517 (2010).
670 19. Puga, M. I. *et al.* SPX1 is a phosphate-dependent inhibitor of Phosphate Starvation
671 Response 1 in Arabidopsis. *Proc. Natl. Acad. Sci. U. S. A.* (2014)
672 doi:10.1073/pnas.1404654111.
673 20. Wang, Z. *et al.* Rice SPX1 and SPX2 inhibit phosphate starvation responses through
674 interacting with PHR2 in a phosphate-dependent manner. *Proc. Natl. Acad. Sci. U. S. A.*
675 (2014) doi:10.1073/pnas.1404680111.
676 21. Shi, J. *et al.* The paralogous SPX3 and SPX5 genes redundantly modulate Pi homeostasis
677 in rice. *J. Exp. Bot.* (2014) doi:10.1093/jxb/ert424.
678 22. Duan, K. *et al.* Characterization of a sub-family of Arabidopsis genes with the SPX
679 domain reveals their diverse functions in plant tolerance to phosphorus starvation. *Plant*
680 *J.* **54**, 965–975 (2008).

681 23. Wang, C. *et al.* Involvement of OsSPX1 in phosphate homeostasis in rice. *Plant J.* **57**,
682 895–904 (2009).
683 24. Wang, Z. *et al.* Regulation of OsSPX1 and OsSPX3 on Expression of OsSPX domain
684 Genes and Pi-starvation Signaling in Rice. *J. Integr. Plant Biol.* **51**, 663–674 (2009).
685 25. Lv, Q. *et al.* SPX4 negatively regulates phosphate signaling and homeostasis through its
686 interaction with PHR2 in rice. *Plant Cell* (2014) doi:10.1105/tpc.114.123208.
687 26. Zhong, Y. *et al.* Rice SPX6 negatively regulates the phosphate starvation response
688 through suppression of the transcription factor PHR2. *New Phytol.* (2018)
689 doi:10.1111/nph.15155.
690 27. Osorio, M. B. *et al.* SPX4 Acts on PHR1-Dependent and -Independent Regulation of
691 Shoot Phosphorus Status in Arabidopsis. *Plant Physiol.* (2019) doi:10.1104/pp.18.00594.
692 28. Qi, W., Manfield, I. W., Muench, S. P. & Baker, A. AtSPX1 affects the AtPHR1–DNA-
693 binding equilibrium by binding monomeric AtPHR1 in solution. *Biochem. J.* **474**, 3675–
694 3687 (2017).
695 29. Ruan, W. *et al.* Two RING-Finger Ubiquitin E3 Ligases Regulate the Degradation of
696 SPX4, An Internal Phosphate Sensor, for Phosphate Homeostasis and Signaling in Rice.
697 *Mol. Plant* (2019) doi:10.1016/j.molp.2019.04.003.
698 30. Jung, J.-Y., Ried, M. K., Hothorn, M. & Poirier, Y. Control of plant phosphate
699 homeostasis by inositol pyrophosphates and the SPX domain. *Curr. Opin. Biotechnol.* **49**,
700 156–162 (2018).
701 31. Wild, R. *et al.* Control of eukaryotic phosphate homeostasis by inositol polyphosphate
702 sensor domains. *Science* (2016) doi:10.1126/science.aad9858.
703 32. Dong, J. *et al.* Inositol Pyrophosphate InsP8 Acts as an Intracellular Phosphate Signal in
704 Arabidopsis. *Mol. Plant* (2019) doi:10.1016/j.molp.2019.08.002.
705 33. Shears, S. B. Intimate connections: Inositol pyrophosphates at the interface of metabolic
706 regulation and cell signaling. *J. Cell. Physiol.* **233**, 1897–1912 (2018).
707 34. Laha, D. *et al.* Arabidopsis ITPK1 and ITPK2 Have an Evolutionarily Conserved Phytic
708 Acid Kinase Activity. *ACS Chem. Biol.* **14**, 2127–2133 (2019).

709 35. Desai, M. *et al.* Two inositol hexakisphosphate kinases drive inositol pyrophosphate
710 synthesis in plants. *Plant J.* **80**, 642–653 (2014).
711 36. Laha, D. *et al.* VIH2 Regulates the Synthesis of Inositol Pyrophosphate InsP8 and
712 Jasmonate-Dependent Defenses in Arabidopsis. *Plant Cell* **27**, 1082–1097 (2015).
713 37. Zhu, J. *et al.* Two bifunctional inositol pyrophosphate kinases/phosphatases control plant
714 phosphate homeostasis. *eLife* (2019) doi:10.7554/elife.43582.
715 38. Couso, I. *et al.* Synergism between Inositol Polyphosphates and TOR Kinase Signaling in
716 Nutrient Sensing, Growth Control, and Lipid Metabolism in Chlamydomonas. *Plant Cell*
717 **28**, 2026–2042 (2016).
718 39. Gu, C. *et al.* The Significance of the Bifunctional Kinase/Phosphatase Activities of
719 Diphosphoinositol Pentakisphosphate Kinases (PPIP5Ks) for Coupling Inositol
720 Pyrophosphate Cell Signaling to Cellular Phosphate Homeostasis. *J. Biol. Chem.* **292**,
721 4544–4555 (2017).
722 40. Pascual-Ortiz, M. *et al.* Asp1 Bifunctional Activity Modulates Spindle Function via
723 Controlling Cellular Inositol Pyrophosphate Levels in Schizosaccharomyces pombe. *Mol.*
724 *Cell. Biol.* **38**, (2018).
725 41. Lorenzo-Orts, L., Couto, D. & Hothorn, M. Identity and functions of inorganic and
726 inositol polyphosphates in plants. *New Phytol.* (2019) doi:10.1111/nph.16129.
727 42. Jiang, M. *et al.* Structural basis for the Target DNA recognition and binding by the MYB
728 domain of phosphate starvation response 1. *FEBS J.* **286**, 2809–2821 (2019).
729 43. Mulugu, S. *et al.* A Conserved Family of Enzymes That Phosphorylate Inositol
730 Hexakisphosphate. *Science* **316**, 106–109 (2007).
731 44. Draškovič, P. *et al.* Inositol Hexakisphosphate Kinase Products Contain Diphosphate and
732 Triphosphate Groups. *Chem. Biol.* **15**, 274–286 (2008).
733 45. Jaillais, Y. *et al.* Tyrosine phosphorylation controls brassinosteroid receptor activation by
734 triggering membrane release of its kinase inhibitor. *Genes Dev.* **25**, 232–237 (2011).
735 46. Holm, L. & Sander, C. Protein structure comparison by alignment of distance matrices. *J.*
736 *Mol. Biol.* **233**, 123–138 (1993).

737 47. Andres, S. N. *et al.* Tetrameric Ctp1 coordinates DNA binding and DNA bridging in
738 DNA double-strand-break repair. *Nat. Struct. Mol. Biol.* **22**, 158–166 (2015).
739 48. Qi, W., Manfield, I. W., Muench, S. P. & Baker, A. AtSPX1 affects the AtPHR1–DNA-
740 binding equilibrium by binding monomeric AtPHR1 in solution. *Biochem. J.* **474**, 3675–
741 3687 (2017).
742 49. Krissinel, E. & Henrick, K. Inference of macromolecular assemblies from crystalline
743 state. *J. Mol. Biol.* **372**, 774–797 (2007).
744 50. Clough, S. J. & Bent, A. F. Floral dip: A simplified method for Agrobacterium-mediated
745 transformation of Arabidopsis thaliana. *Plant J.* (1998) doi:10.1046/j.1365-
746 313X.1998.00343.x.
747 51. Puschmann, R., Harmel, R. K. & Fiedler, D. Scalable Chemoenzymatic Synthesis of
748 Inositol Pyrophosphates. *Biochemistry* **58**, 3927–3932 (2019).
749 52. Kabsch, W. Automatic processing of rotation diffraction data from crystals of initially
750 unknown symmetry land cell constants. *J. Appl. Crystallogr.* (1993)
751 doi:10.1107/S0021889893005588.
752 53. McCoy, A. J. *et al.* Phaser crystallographic software. *J. Appl. Crystallogr.* (2007)
753 doi:10.1107/S0021889807021206.
754 54. Emsley, P. & Cowtan, K. Coot: Model-building tools for molecular graphics. *Acta*
755 *Crystallogr. D Biol. Crystallogr.* (2004) doi:10.1107/S0907444904019158.
756 55. Adams, P. D. *et al.* PHENIX: A comprehensive Python-based system for macromolecular
757 structure solution. *Acta Crystallogr. D Biol. Crystallogr.* (2010)
758 doi:10.1107/S0907444909052925.
759 56. Murshudov, G. N., Vagin, A. A. & Dodson, E. J. Refinement of macromolecular
760 structures by the maximum-likelihood method. *Acta Crystallogr. D Biol. Crystallogr.* **53**,
761 240–255 (1997).
762 57. Davis, I. W. *et al.* MolProbity: All-atom contacts and structure validation for proteins and
763 nucleic acids. *Nucleic Acids Res.* (2007) doi:10.1093/nar/gkm216.
764 58. Goddard, T. D. *et al.* UCSF ChimeraX: Meeting modern challenges in visualization and
765 analysis. *Protein Sci. Publ. Protein Soc.* **27**, 14–25 (2018).

766 59. Bordoli, L. *et al.* Protein structure homology modeling using SWISS-MODEL workspace.
767 *Nat. Protoc.* (2009) doi:10.1038/nprot.2008.197.
768 60. Benkert, P., Künzli, M. & Schwede, T. QMEAN server for protein model quality
769 estimation. *Nucleic Acids Res.* (2009) doi:10.1093/nar/gkp322.
770 61. Notredame, C., Higgins, D. G. & Heringa, J. T-coffee: A novel method for fast and
771 accurate multiple sequence alignment. *J. Mol. Biol.* (2000) doi:10.1006/jmbi.2000.4042.
772 62. Nilsson, L., Müller, R. & Nielsen, T. H. Increased expression of the MYB-related
773 transcription factor, PHR1, leads to enhanced phosphate uptake in Arabidopsis thaliana.
774 *Plant Cell Environ.* (2007) doi:10.1111/j.1365-3040.2007.01734.x.
775 63. Murashige, T. & Skoog, F. A Revised Medium for Rapid Growth and Bio Assays with
776 Tobacco Tissue Cultures. *Physiol. Plant.* (1962) doi:10.1111/j.1399-
777 3054.1962.tb08052.x.
778 64. Ames, B. N. [10] Assay of inorganic phosphate, total phosphate and phosphatases.
779 *Methods Enzymol.* (1966) doi:10.1016/0076-6879(66)08014-5.
780 65. Dong, J. *et al.* Inositol Pyrophosphate InsP8 Acts as an Intracellular Phosphate Signal in
781 Arabidopsis. *Mol. Plant* (2019) doi:10.1016/j.molp.2019.08.002.
782 66. Herberich, E., Sikorski, J. & Hothorn, T. A robust procedure for comparing multiple
783 means under heteroscedasticity in unbalanced designs. *PloS One* **5**, e9788 (2010).
784 67. Dunnett, C. W. A Multiple Comparison Procedure for Comparing Several Treatments
785 with a Control. *J. Am. Stat. Assoc.* **50**, 1096–1121 (1955).
786 68. Gibson, D. G. *et al.* Enzymatic assembly of DNA molecules up to several hundred
787 kilobases. *Nat. Methods* (2009) doi:10.1038/nmeth.1318.
788 69. Liu, H. & Naismith, J. H. An efficient one-step site-directed deletion, insertion, single and
789 multiple-site plasmid mutagenesis protocol. *BMC Biotechnol.* **8**, 91 (2008).
790 70. Binder, A. *et al.* A modular plasmid assembly kit for multigene expression, gene silencing
791 and silencing rescue in plants. *PLoS ONE* (2014) doi:10.1371/journal.pone.0088218.
792 71. Adams, P. D. *et al.* PHENIX: A comprehensive Python-based system for macromolecular
793 structure solution. *Acta Crystallogr. D Biol. Crystallogr.* (2010)
794 doi:10.1107/S0907444909052925.

795 72. Davis, I. W. *et al.* MolProbity: All-atom contacts and structure validation for proteins and
796 nucleic acids. *Nucleic Acids Res.* (2007) doi:10.1093/nar/gkm216.

73. Kabsch, W. & Sander, C. Dictionary of protein secondary structure: pattern recognition of hydrogen-bonded and geometrical features. *Biopolymers* **22**, 2577–2637 (1983).

Acknowledgements

This work was supported by European Research Council Consolidator Grant 818696/INSPIRE (to MH), by Swiss National Foundation Sinergia Grant CRSII5_170925 (to MH and DF), and by an HHMI International Research Scholar Award (to MH). MKR was supported by an EMBO long-term fellowship (ALTF-129-2017). We thank Irene Sabater for providing LI SPX1, and members of the Hothorn lab for critically reading the manuscript.

Author contributions

MKR: Conceptualization, data curation, formal analysis, validation, investigation, visualization, methodology, and writing (original draft, review and editing). RW: Conceptualization, data curation, formal analysis, validation, investigation, methodology, and writing (review and editing). JZ: Investigation, methodology and writing (review and editing). RKH: Methodology. LB: Investigation and methodology. LAH: Software, formal analysis, methodology. DF: Resources, methodology, writing (review and editing). MH: Conceptualization, resources, data curation, formal analysis, supervision, funding acquisition, validation, investigation, visualization, methodology, project administration and writing (original draft, review, and editing).

Conflict of interest

The authors declare no conflict of interest.

Figure legends

Fig. 1 AtSPX1 recognizes the AtPHR1 CC domain that crystallizes as a tetramer.

a Yeast co-expressing different AtPHR1 deletion constructs fused to the Gal4-activation domain (AD; prey) and full-length wild-type AtSPX1 fused to the LexA-binding domain (BD; bait) were grown on selective SD medium supplemented with histidine (+ His; co-transformation control) or lacking histidine (- His; interaction assay) to map a minimal fragment of AtPHR1 sufficient for interaction with AtSPX1. Shown are serial dilutions from left to right. A schematic overview of the tested interacting (in cyan) and non-interacting (in magenta) AtPHR1 fragments is shown alongside (MYB, DNA binding domain; CC, coiled-coil domain). **b** Isothermal titration calorimetry assays of $InsP_7$ (400 µM 5PP-$InsP_5$; left panel) and $InsP_8$ (500 µM 1,5$(PP)_2$-$InsP_4$; right panel) binding to OsSPX4 – OsPHR2 (30 µM), respectively. Raw heats per injection are shown in the top panel, the bottom panel represents the integrated heats of each injection, fitted to a one-site binding model (solid line). The insets show the dissociation constant (K_d) and binding stoichiometry (N) (± fitting error). **c** Ribbon and surface diagrams of the AtPHR1 CC four-stranded anti-parallel tetramer. Helices contributing to the dimer interface are shown in light- and dark-blue, respectively. Corresponding, symmetry-related helices completing the tetramer are shown in light and dark-grey. **d** Structural superposition of two core CC helices from AtPHR1 (C_α trace, in light blue) and ScCtp1 (PDB-ID 4X01, in orange)[47]. R.m.s.d. is ~1 Å comparing 45 corresponding C_α atoms. **e** Ribbon diagram of the ScCtp1 dimer-of-dimers CC domain, with contributing helices colored from yellow to red.

Fig. 2 Mutations in the AtPHR1 CC domain impair oligomerisation and DNA binding.

a Analytical size exclusion chromatography traces of wild type AtPHR1 CC (wt, black line), AtPHR1$^{280-360\ Olig1}$ (Olig 1, cyan), AtPHR1$^{280-360\ Olig2}$ (Olig 2, orange), and of AtPHR1$^{280-360\ KHR}$ (KHR, magenta). The corresponding right-angle light scattering (RALS) traces are shown alongside, the molecular masses are depicted by a black line. Table summaries provide the molecular weight (Mw), retention volume (RV), dispersity (Mw/Mn), and the derived oligomeric state of the respective sample. **b** Analysis of AtPHR1 MYB CC (AtPHR1$^{222-358}$) as described in **a**. **c** Qualitative comparison of the interaction of AtPHR1$^{222-358}$ (upper panel) or AtPHR1$^{222-358\ Olig1}$ (lower panel) binding to IRD800-*pAtSPX1* in electrophoretic mobility shift assays. **d-f**, Quantitative comparison of the interaction of AtPHR1$^{222-358}$, AtPHR1$^{222-358\ Olig1}$, or AtPHR1$^{222-358\ Olig2}$ with *pSPX1* by grating-coupled interferometry (GCI). Sensorgrams show raw data (red lines) and their respective fits (black lines). Table summaries provide the derived association rate (k_a), the dissociation rate (k_d) and the dissociation constant (K_d).

Fig. 3 The KHR motif at the surface of the PHR CC is required for the interaction with SPX domains.

a Ribbon diagram of the AtPHR1 CC domain with conserved basic residues located at the surface of the domain shown in bonds representation. The KHR motif (AtSPX1^{K325}, AtSPX1^{H328}, AtSPX1^{R335}) is highlighted in magenta. **b** Mutational analysis of the basic residues in AtPHR1 CC. Yeast co-expressing AtPHR1$^{226-360}$ variants in which surface exposed basic residues have been replaced with alanine fused to the Gal4-AD (prey) and AtSPX1 fused to the LexA-BD (bait) were grown on selective SD medium supplemented with histidine (+ His; co-transformation control) or lacking histidine and supplemented with 10 mM 3-amini-1,2,4-triazole (3-AT) (- His + 10 mM 3-AT; interaction assay) to identify residues required for interaction with AtSPX1 in yeast two-hybrid assays. Shown are serial

867 dilutions from lift to right. **c** Isothermal titration calorimetry (ITC) assay of wild-type
868 OsPHR2 and OsPHR2^{KHR} (300 µM) versus OsSPX4 (20 µM) - 5PP-InsP$_5$ (100 µM). Raw
869 heats per injection are shown in the top panel, the bottom panel represents the integrated heats
870 of each injection, fitted to a one-site binding model (solid line). The insets show the
871 dissociation constant (K_d) and binding stoichiometry (N) (± fitting error, n.d. no detectable
872 binding). **d** Quantitative comparison of the interaction of OsPHR2 (top panel) or OsPHR2^{KHR}
873 (bottom panel) with *pOsIPS1* by GCI. Sensorgrams show raw data (red lines) and their
874 respective fits (black lines). The insets show summarize association rates (k_a), dissociation
875 rates (k_d) and the dissociation constant (K_d) of the respective sample.
876
877 **Fig. 4** Mutation of the AtPHR1 KHR motif impairs interaction with AtSPX1 and Pi
878 homeostasis *in planta*.
879 **a** Growth phenotypes of Col-0 wild type, *phr1-3* of *phr1-3* complementation lines expressing
880 FLAG-AtPHR1, FLAG-AtPHR1^{K325A}, FLAG-AtPHR1^{H328A}, FLAG-AtPHR1^{R335A}, FLAG-
881 AtPHR1$^{K325A\ R335A}$, and FLAG-AtPHR1$^{K325A\ H328A\ R335A}$ under the control of the *AtPHR1*
882 promoter at 21 DAG grown in Pi sufficient conditions. One representative line per
883 complementation construct is shown (specified by a #), additional lines are shown in
884 Supplementary Fig. 4. **b** Pi content of the lines shown in a. Seedlings were germinated and
885 grown on vertical $^{1/2}$MS plates for 8 d, transferred to $^{1/2}$MS plates supplemented with either 0
886 mM, 1 mM or 10 mM Pi and grown for additional 7 d. For each line, four plants were
887 measured in technical duplicates. Pi contents of all lines can be found in Supplementary Fig.
888 4. **c** Heat maps of PSI marker gene (*ACP5, IPS1, MGD3, PECP1, PPsPase, SPX1*) expression
889 analyses of the lines shown in **a**, represented as Z-scores. For each line, three biological
890 replicates were analysed in technical triplicates by qRT-PCR. **d** Co-immunoprecipitation (Co-
891 IP) experiment assessing the ability for immobilized GFP-AtPHR1 and GFP-AtPHR1$^{KHR/A}$ to
892 interact with mCherry-AtSPX1 in *N. benthamiana*. Input western blots are shown alongside. **e**

893 Genetic interactions in the VIH-PHR signalling pathway. Col-0 wild type and the indicated
894 mutant seedlings were grown on $^{1/2}$MS plates for 7 DAG, transferred to $^{1/2}$MS plates
895 supplemented with either 0 mM, 1 mM or 10 mM Pi and grown for additional 7 d. For
896 complementation analyses, wild-type AtPHR1 or AtPHR1$^{KHR/AAA}$ was expressed as an N-
897 terminal eGFP fusion protein under the control of the *AtPHR1* promoter. **f** Heat maps of PSI
898 marker gene expression for the lines shown in **e**.
899

900 **Supplementary Table 1 – Stable transgenic *A. thaliana* lines.**

Promoter	**N-terminal tag**	**Gene**	**Genetic background**	**Selection**
pPHR1	FLAG	PHR1	phr1-3	p35S:mCherry
pPHR1	FLAG	*PHR1*^{K325A}	phr1-3	p35S:mCherry
pPHR1	FLAG	*PHR1*^{H328A}	phr1-3	p35S:mCherry
pPHR1	FLAG	*PHR1*^{R335A}	phr1-3	p35S:mCherry
pPHR1	FLAG	*PHR1*$^{K325A, R335A}$	phr1-3	p35S:mCherry
pPHR1	FLAG	*PHR1*$^{K325A\ H328A\ R335A}$	phr1-3	p35S:mCherry
pPHR1	eGFP	PHR1	phr1 phl1	hygromycin
pPHR1	eGFP	PHR1$^{K325A\ H328A\ R335A}$	phr1 phl1	hygromycin

901

902 **Supplementary Table 2 – Yeast strains.**

903 Plasmids for yeast transformation have been generated via Gibson cloning[68]. Mutations
904 targeting AtPHR1 K325, H328 and R335 were introduced by site-directed mutagenesis
905 PCR[69].

Strain	**Plasmids**	**Genotype**
TATA	untransformed	gal4::loxP-kanMX-loxP/Gal4D, ade2 trp1-901/ade2-101::loxP-kanMX-loxP, leu2-3,112/ leu2-3,-112, his3D200/ his3D200, LYS2/lys2::(lexAop)4-HIS3, ura3-52::URA3(lexAop)8-lacZ/ ura3-52 URA3::UASGAL1-LacZ
TATA	*pB29:AtSPX1*$^{1-252}$	gal4::loxP-kanMX-loxP/Gal4D, ade2 trp1-901/ade2-101::loxP-

	pP6:AtPHR1$^{1-409}$	kanMX-loxP, leu2-3,112/ leu2-3,-112, his3D200/ his3D200, LYS2/lys2::(lexAop)4-HIS3, ura3-52::URA3(lexAop)8-lacZ/ ura3-52 URA3::UASGAL1-LacZ, pB29-pADH1-AtSPX1-LexA-tADH1-TRP1-TetR, pP6-pADH1-Gal4_AD-AtPHR_1-1227-tADH1-LEU2-ampR
TATA	*pB29:AtSPX1*$^{1-252}$ *pP6:AtPHR1*$^{226-360}$	gal4::loxP-kanMX-loxP/Gal4D, ade2 trp1-901/ade2-101::loxP-kanMX-loxP, leu2-3,112/ leu2-3,-112, his3D200/ his3D200, LYS2/lys2::(lexAop)4-HIS3, ura3-52::URA3(lexAop)8-lacZ/ ura3-52 URA3::UASGAL1-LacZ, pB29-pADH1-AtSPX1-LexA-tADH1-TRP1-TetR, pP6-pADH1-Gal4_AD-AtPHR_678-1080-tADH1-LEU2-ampR
TATA	*pB29:AtSPX1*$^{1-252}$ *pP6:AtPHR1*$^{280-360}$	gal4::loxP-kanMX-loxP/Gal4D, ade2 trp1-901/ade2-101::loxP-kanMX-loxP, leu2-3,112/ leu2-3,-112, his3D200/ his3D200, LYS2/lys2::(lexAop)4-HIS3, ura3-52::URA3(lexAop)8-lacZ/ ura3-52 URA3::UASGAL1-LacZ, pB29-pADH1-AtSPX1-LexA-tADH1-TRP1-TetR, pP6-pADH1-Gal4_AD-PHR_840-1080-tADH1-LEU2-ampR
TATA	*pB29:AtSPX1*$^{1-252}$ *pP6:AtPHR1*$^{300-360}$	gal4::loxP-kanMX-loxP/Gal4D, ade2 trp1-901/ade2-101::loxP-kanMX-loxP, leu2-3,112/ leu2-3,-112, his3D200/ his3D200, LYS2/lys2::(lexAop)4-HIS3, ura3-52::URA3(lexAop)8-lacZ/ ura3-52 URA3::UASGAL1-LacZ, pB29-pADH1-AtSPX1-LexA-tADH1-TRP1-TetR, pP6-pADH1-Gal4_AD-PHR_900-1080-tADH1-LEU2-ampR
TATA	*pB29:AtSPX1*$^{1-252}$ *pP6:AtPHR1*$^{280-353}$	gal4::loxP-kanMX-loxP/Gal4D, ade2 trp1-901/ade2-101::loxP-kanMX-loxP, leu2-3,112/ leu2-3,-112, his3D200/ his3D200, LYS2/lys2::(lexAop)4-HIS3, ura3-52::URA3(lexAop)8-lacZ/ ura3-52 URA3::UASGAL1-LacZ, pB29-pADH1-AtSPX1-LexA-tADH1-TRP1-TetR, pP6-pADH1-Gal4_AD-PHR_840-1059-tADH1-LEU2-ampR
TATA	*pB29:AtSPX1*$^{1-252}$ *pP6:AtPHR1*$^{280-342}$	gal4::loxP-kanMX-loxP/Gal4D, ade2 trp1-901/ade2-101::loxP-kanMX-loxP, leu2-3,112/ leu2-3,-112, his3D200/ his3D200, LYS2/lys2::(lexAop)4-HIS3, ura3-52::URA3(lexAop)8-lacZ/ ura3-52 URA3::UASGAL1-LacZ, pB29-pADH1-AtSPX1-LexA-tADH1-TRP1-TetR, pP6-pADH1-Gal4_AD-PHR_840-1026-tADH1-LEU2-ampR
TATA	*pB29:AtSPX1*$^{1-252}$ *pP6:AtPHR1*$^{1-225}$	gal4::loxP-kanMX-loxP/Gal4D, ade2 trp1-901/ade2-101::loxP-kanMX-loxP, leu2-3,112/ leu2-3,-112, his3D200/ his3D200, LYS2/lys2::(lexAop)4-HIS3, ura3-52::URA3(lexAop)8-lacZ/ ura3-52 URA3::UASGAL1-LacZ, pB29-pADH1-AtSPX1-LexA-tADH1-TRP1-TetR, pP6-pADH1-Gal4_AD-PHR_1-675-tADH1-LEU2-ampR
TATA	*pB29:AtSPX1*$^{1-252}$ *pP6:AtPHR1*$^{360-409}$	gal4::loxP-kanMX-loxP/Gal4D, ade2 trp1-901/ade2-101::loxP-kanMX-loxP, leu2-3,112/ leu2-3,-112, his3D200/ his3D200, LYS2/lys2::(lexAop)4-HIS3, ura3-52::URA3(lexAop)8-lacZ/ ura3-52 URA3::UASGAL1-LacZ, pB29-pADH1-AtSPX1-LexA-tADH1-TRP1-TetR, pP6-pADH1-Gal4_AD-PHR_1080-1227-tADH1-LEU2-ampR
TATA	*pB29 AtSPX2*$^{1-287}$ *pP6:AtPHR1*$^{226-360}$	gal4::loxP-kanMX-loxP/Gal4D, ade2 trp1-901/ade2-101::loxP-kanMX-loxP, leu2-3,112/ leu2-3,-112, his3D200/ his3D200, LYS2/lys2::(lexAop)4-HIS3, ura3-52::URA3(lexAop)8-lacZ/ ura3-52 URA3::UASGAL1-LacZ, pB29-pADH1-AtSPX2_1-861-LexA-tADH1-TRP1-TetR, pP6-pADH1-Gal4_AD-AtPHR_678-1080-tADH1-LEU2-ampR
TATA	*pB29:AtSPX3*$^{1-245}$	gal4::loxP-kanMX-loxP/Gal4D, ade2 trp1-901/ade2-101::loxP-

	pP6:AtPHR1$^{226\text{-}360}$	kanMX-loxP, leu2-3,112/ leu2-3,-112, his3D200/ his3D200, LYS2/lys2::(lexAop)4-HIS3, ura3-52::URA3(lexAop)8-lacZ/ ura3-52 URA3::UASGAL1-LacZ, pB29-pADH1-AtSPX3_1-735-LexA-tADH1-TRP1-TetR, pP6-pADH1-Gal4_AD-AtPHR_678-1080-tADH1-LEU2-ampR
TATA	*pB29:AtSPX4*$^{1\text{-}318}$ *pP6:AtPHR1*$^{226\text{-}360}$	gal4::loxP-kanMX-loxP/Gal4D, ade2 trp1-901/ade2-101::loxP-kanMX-loxP, leu2-3,112/ leu2-3,-112, his3D200/ his3D200, LYS2/lys2::(lexAop)4-HIS3, ura3-52::URA3(lexAop)8-lacZ/ ura3-52 URA3::UASGAL1-LacZ, pB29-pADH1-AtSPX4_1-954-LexA-tADH1-TRP1-TetR, pP6-pADH1-Gal4_AD-AtPHR_678-1080-tADH1-LEU2-ampR
TATA	*pB29:AtSPX1*$^{1\text{-}252\ PBC}$ *pP6:AtPHR1*$^{226\text{-}360}$	gal4::loxP-kanMX-loxP/Gal4D, ade2 trp1-901/ade2-101::loxP-kanMX-loxP, leu2-3,112/ leu2-3,-112, his3D200/ his3D200, LYS2/lys2::(lexAop)4-HIS3, ura3-52::URA3(lexAop)8-lacZ/ ura3-52 URA3::UASGAL1-LacZ, pB29-pADH1-AtSPX1_Y25F_K29A_K140A-LexA-tADH1-TRP1-TetR, pP6-pADH1-Gal4_AD-PHR_678-1080-tADH1-LEU2-ampR
TATA	*pB29:AtSPX1*$^{1\text{-}252\ KSC}$ *pP6:AtPHR1*$^{226\text{-}360}$	gal4::loxP-kanMX-loxP/Gal4D, ade2 trp1-901/ade2-101::loxP-kanMX-loxP, leu2-3,112/ leu2-3,-112, his3D200/ his3D200, LYS2/lys2::(lexAop)4-HIS3, ura3-52::URA3(lexAop)8-lacZ/ ura3-52 URA3::UASGAL1-LacZ, pB29-pADH1-AtSPX1_K136A_K139A_K143A-LexA-tADH1-TRP1-TetR, pP6-pADH1-Gal4_AD-PHR_678-1080-tADH1-LEU2-ampR
TATA	*pB29:AtSPX1*$^{1\text{-}252\ K81A}$ *pP6:AtPHR1*$^{226\text{-}360}$	gal4::loxP-kanMX-loxP/Gal4D, ade2 trp1-901/ade2-101::loxP-kanMX-loxP, leu2-3,112/ leu2-3,-112, his3D200/ his3D200, LYS2/lys2::(lexAop)4-HIS3, ura3-52::URA3(lexAop)8-lacZ/ ura3-52 URA3::UASGAL1-LacZ, pB29-pADH1-AtSPX1_K81A-LexA-tADH1-TRP1-TetR, pP6-pADH1-Gal4_AD-PHR_678-1080-tADH1-LEU2-ampR
TATA	*pB29:AtSPX1*$^{1\text{-}252}$ *pP6:AtPHR1*$^{226\text{-}360\ K308A}$	gal4::loxP-kanMX-loxP/Gal4D, ade2 trp1-901/ade2-101::loxP-kanMX-loxP, leu2-3,112/ leu2-3,-112, his3D200/ his3D200, LYS2/lys2::(lexAop)4-HIS3, ura3-52::URA3(lexAop)8-lacZ/ ura3-52 URA3::UASGAL1-LacZ, pB29-pADH1-AtSPX1-LexA-tADH1-TRP1-TetR, pP6-pADH1-Gal4_AD-PHR_678-1080_K308A-tADH1-LEU2-ampR
TATA	*pB29:AtSPX1*$^{1\text{-}252}$ *pP6:AtPHR1*$^{226\text{-}360\ R318A}$	gal4::loxP-kanMX-loxP/Gal4D, ade2 trp1-901/ade2-101::loxP-kanMX-loxP, leu2-3,112/ leu2-3,-112, his3D200/ his3D200, LYS2/lys2::(lexAop)4-HIS3, ura3-52::URA3(lexAop)8-lacZ/ ura3-52 URA3::UASGAL1-LacZ, pB29-pADH1-AtSPX1-LexA-tADH1-TRP1-TetR, pP6-pADH1-Gal4_AD-PHR_678-1080_R318A-tADH1-LEU2-ampR
TATA	*pB29:AtSPX1*$^{1\text{-}252}$ *pP6:AtPHR1*$^{226\text{-}360\ K325A}$	gal4::loxP-kanMX-loxP/Gal4D, ade2 trp1-901/ade2-101::loxP-kanMX-loxP, leu2-3,112/ leu2-3,-112, his3D200/ his3D200, LYS2/lys2::(lexAop)4-HIS3, ura3-52::URA3(lexAop)8-lacZ/ ura3-52 URA3::UASGAL1-LacZ, pB29-pADH1-AtSPX1-LexA-tADH1-TRP1-TetR, pP6-pADH1-Gal4_AD-PHR_678-1080_K325A-tADH1-LEU2-ampR
TATA	*pB29:AtSPX1*$^{1\text{-}252}$ *pP6:AtPHR1*$^{226\text{-}360\ H328A}$	gal4::loxP-kanMX-loxP/Gal4D, ade2 trp1-901/ade2-101::loxP-kanMX-loxP, leu2-3,112/ leu2-3,-112, his3D200/ his3D200, LYS2/lys2::(lexAop)4-HIS3, ura3-52::URA3(lexAop)8-lacZ/ ura3-52 URA3::UASGAL1-LacZ, pB29-pADH1-AtSPX1-LexA-tADH1-TRP1-TetR, pP6-pADH1-Gal4_AD-PHR_678-1080_H328A-tADH1-LEU2-ampR
TATA	*pB29:AtSPX1*$^{1\text{-}252}$	gal4::loxP-kanMX-loxP/Gal4D, ade2 trp1-901/ade2-101::loxP-

	pP6:AtPHR1$^{226\text{-}360\ R335A}$	kanMX-loxP, leu2-3,112/ leu2-3,-112, his3D200/ his3D200, LYS2/lys2::(lexAop)4-HIS3, ura3-52::URA3(lexAop)8-lacZ/ ura3-52 URA3::UASGAL1-LacZ, pB29-pADH1-AtSPX1-LexA-tADH1-TRP1-TetR, pP6-pADH1-Gal4_AD-PHR_678-1080_R335A-tADH1-LEU2-ampR
TATA	*pB29:AtSPX1*$^{1\text{-}252}$ *pP6:AtPHR1*$^{226\text{-}360\ K325A\ R335A}$	gal4::loxP-kanMX-loxP/Gal4D, ade2 trp1-901/ade2-101::loxP-kanMX-loxP, leu2-3,112/ leu2-3,-112, his3D200/ his3D200, LYS2/lys2::(lexAop)4-HIS3, ura3-52::URA3(lexAop)8-lacZ/ ura3-52 URA3::UASGAL1-LacZ, pB29-pADH1-AtSPX1-LexA-tADH1-TRP1-TetR, pP6-pADH1-Gal4_AD-PHR_678-1080_ K325AR335A -tADH1-LEU2-ampR
TATA	*pB29:AtSPX1*$^{1\text{-}252}$ *pP6:AtPHR1*$^{226\text{-}360\ K325A\ H328A\ R335A}$	gal4::loxP-kanMX-loxP/Gal4D, ade2 trp1-901/ade2-101::loxP-kanMX-loxP, leu2-3,112/ leu2-3,-112, his3D200/ his3D200, LYS2/lys2::(lexAop)4-HIS3, ura3-52::URA3(lexAop)8-lacZ/ ura3-52 URA3::UASGAL1-LacZ, pB29-pADH1-AtSPX1-LexA-tADH1-TRP1-TetR, pP6-pADH1-Gal4_AD-PHR_678-1080_K325AH328AR335A-tADH1-LEU2-ampR
TATA	*pB29:AtSPX1*$^{1\text{-}252}$ *pP6:AtPHR1*$^{226\text{-}360\ R340A}$	gal4::loxP-kanMX-loxP/Gal4D, ade2 trp1-901/ade2-101::loxP-kanMX-loxP, leu2-3,112/ leu2-3,-112, his3D200/ his3D200, LYS2/lys2::(lexAop)4-HIS3, ura3-52::URA3(lexAop)8-lacZ/ ura3-52 URA3::UASGAL1-LacZ, pB29-pADH1-AtSPX1-LexA-tADH1-TRP1-TetR, pP6-pADH1-Gal4_AD-PHR_678-1080_R340A-tADH1-LEU2-ampR
L40	untransformed	MATa ade2 trp1-901 leu2-3,112 lys2-801am his3D200 lys2::(lexAop)4-HIS3, ura3-52::URA3 (lexAop)8-lacZa
L40 ΔVIP1	untransformed	MATa ade2 trp1-901 leu2-3,112 lys2-801am his3D200 lys2::(lexAop)4-HIS3 ura3-52::URA3 (lexAop)8-lacZa vip1::natNT2
L40 ΔKCS1	untransformed	MATa ade2 trp1-901 leu2-3,112 lys2-801am his3D200 lys2::(lexAop)4-HIS3, ura3-52::URA3 (lexAop)8-lacZa kcs1::natNT2
L40	*pB29:AtSPX1*$^{1\text{-}252}$ *pP6:AtPHR1*$^{226\text{-}360}$	MATa ade2 trp1-901 leu2-3,112 lys2-801am his3D200 lys2::(lexAop)4-HIS3, ura3-52::URA3 (lexAop)8-lacZa pB29-pADH1-AtSPX1-LexA-tADH1-TRP1-TetR, pP6-pADH1-Gal4_AD-AtPHR_678-1080-tADH1-LEU2-ampR
L40 ΔVIP1	*pB29:AtSPX1*$^{1\text{-}252}$ *pP6:AtPHR1*$^{226\text{-}360}$	MATa ade2 trp1-901 leu2-3,112 lys2-801am his3D200 lys2::(lexAop)4-HIS3, ura3-52::URA3 (lexAop)8-lacZa vip1::natNT2 pP6-pADH1-Gal4_ADAtPHR_678-1080-tADH1-LEU2-ampR pB29-pADH1-AtSPX1-LexA-tADH1-TRP1-TetR
L40 ΔKCS1	*pB29:AtSPX1*$^{1\text{-}252}$ *pP6:AtPHR1*$^{226\text{-}360}$	MATa ade2 trp1-901 leu2-3,112 lys2-801am his3D200 lys2::(lexAop)4-HIS3, ura3-52::URA3 (lexAop)8-lacZa kcs1::natNT2 pP6-pADH1-Gal4_ADAtPHR_678-1080-tADH1-LEU2-ampR pB29-pADH1-AtSPX1-LexA-tADH1-TRP1-TetR
L40	*pB29:AtBRI1*$^{828\text{-}1196}$ *pP6:AtBKI1*$^{1\text{-}337}$	MATa ade2 trp1-901 leu2-3,112 lys2-801am his3D200 lys2::(lexAop)4-HIS3, ura3-52::URA3 (lexAop)8-lacZa pP6-pADH1-Gal4_AD_pP6_AtBKI1_1-1011-tADH1-LEU2-ampR pB29-pADH1-AtBRI1_2484-3588-LexA-tADH1-TRP1-TetR
L40 ΔVIP1	*pB29:AtBRI1*$^{828\text{-}1196}$ *pP6:AtBKI1*$^{1\text{-}337}$	MATa ade2 trp1-901 leu2-3,112 lys2-801am his3D200 lys2::(lexAop)4-HIS3, ura3-52::URA3 (lexAop)8-lacZa vip1::natNT2 pP6-pADH1-Gal4_AD_pP6_AtBKI1_1-1011-tADH1-LEU2-ampR pB29-pADH1-AtBRI1_2484-3588-LexA-tADH1-TRP1-TetR
L40	*pB29:AtBRI1*$^{828\text{-}1196}$	MATa ade2 trp1-901 leu2-3,112 lys2-801am his3D200 lys2::

ΔKCS1	*pP6:AtBKI1*$^{1\text{-}337}$	(lexAop)4-HIS3 ura3-52::URA3 (lexAop)8-lacZa kcs1::natNT2 pP6-pADH1-Gal4_AD_pP6_AtBKI1_1-1011-tADH1-LEU2-ampR pB29-pADH1-AtBRI1_2484-3588-LexA-tADH1-TRP1-TetR

906

907 **Supplementary Table 3 – Constructs and primers.**

908 **a, Golden Gate Level 0 constructs and primers.** The *PHR1* promoter and gene were
909 amplified from *A. thaliana* gDNA, and *SPX1* was amplified from *A. thaliana* cDNA. Level 0
910 constructs were generated via StuI or SmaI cut-ligation into pUC Amp[70].

Name	**Primer**	**Sequences**
pPHR1.1	OutFwdProm InRevProm	ACGAAGACGTTACGGGTCTCTGCGGATTTTGTAAAACTATG AATC AGGAAGACGGAAAACGAATCGAATCGGAGAAAATG
pPHR1.2	InFwdProm OutRevProm	ATGAAGACCGTTTTCCTTGGTCCTGGATTGCATGAAGACAC CAGAGGTCTCTCAGA TGTTGTCCTGCAAGAGAGAATC
PHR1.1	OutFwdGene InRevGene1	AAGAAGACTCTACGGGTCTCCCACCATGGAGGCTCGTCCAG TTCATAGATCAGGTTCGAGGGACC GCGAAGACTTTTGGTCCTAAAAAAGTGTGTCCAG
PHR1.2	InFwdGene1 InRevGene2	TTGAAGACGACCAAAAGACACTGCAAATTCCGCAACC TAGAAGACGAAGCCAATTATATGCATTAGCAGG
PHR1.3	InFwdGene2 InRevGene3	GCGAAGACTTGGCTTCTAATATTAGATTGTG TTGAAGACTCCTCTTGTTCAGATTTGGCTGCGGA
PHR1.4	InFwdGene3 OutRevGene	AAGAAGACCAAGAGGACAAGAAAACTGCTGATTCG ATGAAGACAACAGAGGTCTCTCCTTATTATCGATTTTGGGA CGC
PHR1^{K325A} *a* *PHR1*$^{K325A\ R335A}$ *a* *PHR1*$^{K325A\ H328A\ R335A}$ *a*	InFwdGene2 InRevKA	GCGAAGACTTGGCTTCTAATATTAGATTGTG CAGAAGACTGCGCCTGTACTTCCATCTGAAGTCG
PHR1^{K325A} *b*	InFwdKA InRevGene3	GTGAAGACACGGCGCAACTCCATGAGCAGCTCGAG TTGAAGACTCCTCTTGTTCAGATTTGGCTGCGGA
PHR1^{H328A} *a*	InFwdGene2 InRevHA	GCGAAGACTTGGCTTCTAATATTAGATTGTG CGGAAGACTCAGCGAGTTGCTTCTGTACTTCC
PHR1^{H328A} *b*	InFwdHA InRevGene3	AGGAAGACCTCGCTGAGCAGCTCGAGGTATGTTC TTGAAGACTCCTCTTGTTCAGATTTGGCTGCGGA
PHR1^{R335A} *a*	InFwdGene2 InRevRA	GCGAAGACTTGGCTTCTAATATTAGATTGTG GTGAAGACTTTGCTTGAATCTGCAGGCAAAGG
PHR1^{R335A} *b* *PHR1*$^{K325A\ R335A}$ *c* *PHR1*$^{K325A\ H328A\ R335A}$ *c*	InFwdRA InRevGene3	TAGAAGACCAAGCAAACCTGCAACTCCGAATAGAAG TTGAAGACTCCTCTTGTTCAGATTTGGCTGCGGA
PHR1$^{K325A\ R335A}$ *b*	InFwdKA InRevRA	GTGAAGACACGGCGCAACTCCATGAGCAGCTCGAG GTGAAGACTTTGCTTGAATCTGCAGGCAAAGG
PHR1$^{K325A\ H328A\ R335A}$ *b*	InFwdKAHA	GTGAAGACACGGCGCAACTCGCTGAGCAGCTCGAG

	InRevRA	GTGAAGACTTTGCTTGAATCTGCAGGCAAAGG
SPX1.1	OutFwdGene InRevGene1	AAGAAGACCATACGGGTCTCGCACCATGAAGTTTGGTAAG AGTC TCGAAGACGTCCTCTAACAATTGGATGAAATTG
SPX1.2	InFwdGene1 InRevGene2	CCGAAGACTAGAGGACGAGTTGGAGAAATTCAAC TCGAAGACTGGAGACTCTCCATGAACTTATGC
SPX1.3	InFwdGene2 OutRevGene	TCGAAGACAGTCTCCATATGAAGAGCACAATCGC AGGAAGACTGCAGAGGTCTCACCTTTTTGGCTTCTTGCTCC AAC

911

912 **b, Level I, II & III constructs.** Level 1 and level 3 constructs were generated via BpiI cut-

913 ligation, and level 2 constructs via BsaI cut-ligation[70].

Name	**Assembly**	**Purpose**
LI BpiI pPHR1	pPHR1.1 + pPHR1.2	Cloning
LI BpiI PHR1	PHR1.1 + PHR1.2 + PHR1.3 + PHR1.4	Cloning
LI BpiI PHR1^{K}	PHR1.1 + PHR1.2 + PHR1^{K325A} a + PHR1^{K325A} b + PHR1.4	Cloning
LI BpiI PHR1^{H}	PHR1.1 + PHR1.2 + PHR1^{H328A} a + PHR1^{H328A} b + PHR1.4	Cloning
LI BpiI PHR1^{R}	PHR1.1 + PHR1.2 + PHR1^{R335A} a + PHR1^{R335A} b + PHR1.4	Cloning
LI BpiI PHR1^{KR}	PHR1.1 + PHR1.2 + PHR1$^{K325A\ R335A}$ a + PHR1$^{K325A\ R335A}$ b + PHR1$^{K325A\ R335A}$ c + PHR1.4	Cloning
LI BpiI PHR1^{KHR}	PHR1.1 + PHR1.2 + PHR1$^{K325A\ H328A\ R335A}$ a + PHR1$^{K325A\ H328A\ R335A}$ b + PHR1$^{K325A\ H328A\ R335A}$ c + PHR1.4	Cloning
LI SPX1	SPX1.1 + SPX1.2 + SPX1.3	Cloning
LII R5-6 pPHR1:FLAG-PHR1	LI A-B pPHR1 + LI FLAG B-C + LI C-D PHR1 + LI dy D-E + LI E-F nos-T + LI dy F-G	Cloning
LII R5-6 pPHR1:FLAG-PHR1^{K}	LI A-B pPHR1 + LI FLAG B-C + LI C-D PHR1^{K} + LI dy D-E + LI E-F nos-T + LI dy F-G	Cloning
LII R5-6 pPHR1:FLAG-PHR1^{H}	LI A-B pPHR1 + LI FLAG B-C + LI C-D PHR1^{H} + LI dy D-E + LI E-F nos-T + LI dy F-G	Cloning
LII R5-6 pPHR1:FLAG-PHR1^{R}	LI A-B pPHR1 + LI FLAG B-C + LI C-D PHR1^{R} + LI dy D-E + LI E-F nos-T + LI dy F-G	Cloning
LII R5-6 pPHR1:FLAG-PHR1^{KR}	LI A-B pPHR1 + LI FLAG B-C + LI C-D PHR1^{KR} + LI dy D-E + LI E-F nos-T + LI dy F-G	Cloning
LII R5-6 pPHR1:FLAG-PHR1^{KHR}	LI A-B pPHR1 + LI FLAG B-C + LI C-D PHR1^{KHR} + LI dy D-E + LI E-F nos-T + LI dy F-G	Cloning
LII F1-2 p35S:mCherry	LI A-B p35S + LI dy B-C + LI C-D mCherry + LI dy D-E + LI E-F 35S-T + LI dy F-G	Cloning / *N. benthamiana* transformation
LII F1-2 p35S:mCherry-SPX1	LI A-B p35S + LI mCherry B-C + LI C-D SPX1 + LI dy D-E + LI E-F nos-T + LI dy F-G	*N. benthamiana* transformation

LII F1-2 p35S:GFP-PHR1	LI A-B p35S + LI GFP B-C + LI C-D PHR1 + LI dy D-E + LI E-F nos-T + LI dy F-G	*N. benthamiana* transformation
LII F1-2 p35S:GFP-PHR1^{KHR}	LI A-B p35S + LI GFP B-C + LI C-D PHR1^{KHR} + LI dy D-E + LI E-F nos-T + LI dy F-G	*N. benthamiana* transformation
LIIIβ fin p35S:mCherry pPHR1:FLAG-PHR1	LII p35S:mCherry 1-2 + LII ins 2-3 + LII dy 3-4 + LII ins 4-5 + LII F LII pPHR1:FLAG-PHR1 5-6	*A. thaliana* transformation
LIIIβ fin p35S:mCherry pPHR1:FLAG-PHR1^{K}	LII p35S:mCherry 1-2 + LII ins 2-3 + LII dy 3-4 + LII ins 4-5 + LII F LII pPHR1:FLAG-PHR1 **^{K}** 5-6	*A. thaliana* transformation
LIIIβ fin p35S:mCherry pPHR1:FLAG-PHR1^{H}	LII p35S:mCherry 1-2 + LII ins 2-3 + LII dy 3-4 + LII ins 4-5 + LII F LII pPHR1:FLAG-PHR1 **^{H}** 5-6	*A. thaliana* transformation
LIIIβ fin p35S:mCherry pPHR1:FLAG-PHR1^{R}	LII p35S:mCherry 1-2 + LII ins 2-3 + LII dy 3-4 + LII ins 4-5 + LII F LII pPHR1:FLAG-PHR1 **^{R}** 5-6	*A. thaliana* transformation
LIIIβ fin p35S:mCherry pPHR1:FLAG-PHR1^{KR}	LII p35S:mCherry 1-2 + LII ins 2-3 + LII dy 3-4 + LII ins 4-5 + LII F LII pPHR1:FLAG-PHR1 **^{KR}** 5-6	*A. thaliana* transformation
LIIIβ fin p35S:mCherry pPHR1:FLAG-PHR1^{KHR}	LII p35S:mCherry 1-2 + LII ins 2-3 + LII dy 3-4 + LII ins 4-5 + LII F LII pPHR1:FLAG-PHR1 **^{KHR}** 5-6	*A. thaliana* transformation

c, Plasmids for recombinant protein expression in *E. coli.*

Plasmids for recombinant protein expression in *E. coli* have been generated via Gibson cloning[68]. Mutations targeting AtPHR1 K325, H328 and R335 were introduced by site-directed mutagenesis PCR[69].

Vector	**Construct**	**Purpose**
pMH_HT	*AtPHR1$^{222-358}$*	OmniSEC, GCI, EMSA
pMH_HT	*AtPHR1$^{222-358\ Olig1}$*	OmniSEC, GCI, EMSA
pMH_HT	*AtPHR1$^{222-358\ Olig2}$*	OmniSEC, GCI, EMSA
pMH_HT	*AtPHR1$^{280-360}$*	OmniSEC
pMH_HT	*AtPHR1$^{280-360\ Olig1}$*	OmniSEC
pMH_HT	*AtPHR1$^{280-360\ Olig2}$*	OmniSEC
pMH_HT	*AtPHR1$^{280-360\ K325A,\ H328A,\ R335A}$*	OmniSEC
pMH_HSgb1T	*OsPHR2$^{1-426}$*	OmniSEC, GCI, ITC
pMH_HSgb1T	*OsPHR2$^{1-426\ KHR}$*	OmniSEC, GCI, ITC
pMH_Hssumo	*OsSPX4$^{1-321}$*	ITC
pMH_Hssumo	*AtPHR1$^{280-360}$*	Crystallisation

d, Characterisation of T-DNA mutants.

Name	**5'-3' Sequence**

LBb1.3	ATTTTGCCGATTTCGGAAC
LP_PHR1	GAGAGACCTCACACGCACTTC
RP_PHR1	CTTTCTGGCGAACCTGTAGTG
phl1-LP	GTGGAGACGTTTCTGCACTTC
phl1-RP	TCCCACAATCCAAATTCAGAG

920

921 **e, Gene expression analysis.**

Gene identifier	**Name**	**Sequence**
At3g18780	Actin2_F	AGTGGTCGTACAACCGGTATTGT
	Actin2_R	GATGGCATGGAGGAAGAGAGAAAC
At4g28610	PHR1_F	GTTCAGCAGCAACCTTCTCC
	PHR1_R	GCTCTTTCACTACCGCCAAG
At1g23010	LPR1_F	CCGGGCTATGTCTACCATTGTCAC
	LPR1_R	GCACCATCAAAACTTCGCAGAGATCG
At3g52820	ACP5_F	CAGTTTCTAACTAGTGGTGCTGGA
	ACP5_R	GCTTGGGATTGATGGTCACT
At3g09922	IPS1_F	TGAAGACTGCAGAAGGCTGA
	IPS1_R	CGAAGCTTGCCAAAGGATAG
At2g11810	MGD3_F	AGAGGCCGGTTTAATGGAGT
	MGD3_R	CATCAGAGGATGCACGCTAA
At1g52940	PAP5_F	TCGAACCCGAAAGGCCAAGCGGTGC
	PAP5_R	GCGCTTGGTTCCACAAACCGGCCGTA
At2g38940	PHT1;4_F	CCTCGGTCGTATTTATTACCACG
	PHT1;4_R	CCATCACAGCTTTTGGCTCATG
At5g20150	SPX1_F	CGGGTTTTGAAGGAGATCAG
	SPX1_R	GCGGCAATGAAAACACACTA

922 **f, Primers used for cloning PHR1 into the pH7m34GW vector.**

Name	**5'-3' Sequence**
PHR1_B2F	GGGGACAGCTTTCTTGTACAAAGTGGATGAGGCTCGTCCAGTTCATAG
PHR1_B3R	GGGGACAACTTTGTATAATAAAGTTGATCAATTATCGATTTTGGGACG
eGFP_B1F	GGGGACAAGTTTGTACAAAAAAGCAGGCTTAATGGTGAGCAAGGGCGA

	GGAGCTG
eGFP_B2R	GGGGACCACTTTGTACAAGAAAGCTGGGTACTTGTACAGCTCGTCCATG CC
PHR1_H328A_F	CAACTCGCTGAGCAGCTCGAAATTCAAGCAAACCTGCAACTCCG
PHR1_H328A_R	AGCTGCTCAGCGAGTTGCGCCTGTACTTCCATCTGAAGTCGTAGA
PHR1_R335A_F	ATTCAAGCAAACCTGCAACTCCGAATAGAAGAACAAGG
PHR1_R335A_R	CAGGTTTGCTTGAATTTCGAGCTGCTCATGGAG
PHR1_K325A_F	GTACAGGCGCAACTCCATGAGCAGCTCAGAAATT
PHR1_K325A_R	GAGTTGCGCCTGTACTTCCATCTGAAGTCGTAGAGC

923

924 **Tabel 4 – Modified DNA oligos.**

925 The P1BS (GNATATNC) is shown in bold.

926 **a, IRdye end-labelled oligos for EMSA.**

Name	**Sequence**
AtSPX1_800 _F	5'-IRD800-CAG AGA AAA AA**G GAT ATT C**TA ATT AGA AAC CTT AA**G AAT ATT C**TT TTT AAT CCC-3'
AtSPX1_800_R	5'-IRD800-GGG ATT AAA AA**G AAT ATT C**TT AAG GTT TCT AAT TA**G AAT ATC C**TT TTT TCT CTG-3'

927 **b, Biotinylated oligos for GCI.**

Name	**Sequence**
AtSPX1_Biotin_F	5'-Biotin-CAG AGA AAA AA**G GAT ATT C**TA ATT AGA AAC CTT AA**G AAT ATT C**TT TTT AAT CCC-3'
AtSPX1_R	5'-GGG ATT AAA AA**G AAT ATT** CTT AAG GTT TCT AAT TA**G AAT ATC** CTT TTT TCT CTG-3'
OsIPS1_Biotin_F	5'-Biotin-TAA TGC TCG CC**G CAT ATC** CTT TGG TAG ATA-3'
OsIPS1_R	5'-TAT CTA CCA AAG **GAT ATG C**GG CGA GCA TTA-3'

928

Supplementary Table 5 – Crystallographic data collection and refinement statistics.

	AtPHR1$^{280-360}$ form1	**AtPHR1$^{280-360}$ form2**	**AtPHR1$^{280-360}$ form3**
PDB-ID	**6TO5**	**6TO9**	**6TOC**
Data collection			
Space group	P 6_1 2 2	P 3_2 2 1	P 4_2
Cell dimensions			
a, *b*, *c* (Å)	70.4, 70,4, 148.88	70.05, 70.05, 80.17	31.52, 31.52, 81.60
α, β, γ (°)	90, 90, 120	90, 90, 120	90, 90, 90
Resolution (Å)	47.18 – 2.38 (2.52 – 2.38)	48.37 – 2.45 (2.59 – 2.44)	31.52 – 1.85 (1.97 – 1.85)
R_{meas}[#]	0.189 (2.21)	0.164 (2.77)	0.073 (2.76)
CC(1/2)[#]	0.99 (0.69)	0.99 (0.51)	1.0 (0.40)
$I/\sigma I$[#]	14.85 (1.48)	15.86 (1.07)	21.41 (0.98)
Completeness (%)[#]	99.8 (98.9)	99.3 (96.0)	99.9 (99.3)
Redundancy[#]	20.8 (20.2)	19.0 (18.4)	13.5 (13.4)
Wilson B-factor[#]	56.7	67.8	47.1
Refinement			
Resolution (Å)	41.18 – 2.38	48.37 – 2.45	31.52 – 1.85
No. reflections	16,560	8,702	6,433
R_{work}/ R_{free}[$]	0.22 (0.23)	0.23 (0.26)	0.21 (0.26)
No. atoms			
protein	940	952	753
solvent	18	4	27
Res. B-factors[$]			
protein	64.6	79.1	41.3
solvent	57.4	59.3	40.7
R.m.s deviations[$]			
bond lengths (Å)	0.89	0.98	1.61
bond angles (°)	0.0047	0.0049	0.012
Ramachandran plot[$]:			
most favored regions (%)	99.08	99.07	98.8
outliers (%)	0	0	0
MolProbity score[$]	1.31	1.19	1.24

[*]as defined in XDS[52]

[+]as defined phenix.refine[71] (form 1, form2) or Refmac5[56] (form 3, using twin laws h,k,l and -k, -h, -l with twin fractions of 0.5, apparent point group was P 4 2 2)

[$]as defined in Molprobity[72]

Supplementary Fig. 1 The AtPHR1 – AtSPX1 interaction in yeast is meditated by PP-InsPs. **a** Yeast-2-hybrid assay. Yeast co-expressing AtPHR1$^{226-360}$ fused to the Gal4-AD (prey) and different AtSPX proteins fused to the LexA-BD (bait) were grown on selective SD medium supplemented with histidine (+ His; co-transformation control) or lacking histidine (- His; interaction assay). Shown are serial dilutions from left to right. **b** (Top panel) Homology model of an AtSPX1$^{1-182}$-$InsP_6$ complex. AtSPX1$^{1-182}$ is shown as blue ribbon diagram and side chains involved in $InsP_6$ binding are highlighted in green (PBC, phosphate binding cluster) and purple (KSC, lysine surface cluster) and depicted in bonds representation. The $InsP_6$ ligand is shown in grey (in bonds representation). (Bottom panel) Yeast co-expressing AtPHR1$^{226-360}$ fused to the Gal4-AD (prey) and different AtSPX1 versions mutated in residues involved in $InsP_6$ binding, or a structural control mutant (SC[31]) fused to the LexA-BD (bait) were grown on selective SD medium supplemented with histidine (+ His; co-transformation control) or lacking histidine and supplemented with 10 mM 3-AT(- His + 3-AT; interaction assay) to investigate the importance of the PP-InsP binding surface in AtSPX1 for the AtSPX1 – AtPHR1 interaction in yeast. **c** Yeast knock-out strains for the PP-InsP biosynthesis enzymes Vip1 or Kcs1 co-expressing either AtPHR1$^{226-360}$ fused to the Gal4-AD (prey) and AtSPX1 fused to the LexA-BD (bait) (upper panel), or AtBKI1 fused to the Gal4-AD (prey) and AtBRI1 fused to the LexA-BD (bait) (lower panel) were grown on selective SD medium supplemented with histidine (+ His; co-transformation control) or lacking histidine and supplemented with 10 mM 3-AT (- His + 3-AT; interaction assay) to investigate the importance of the availability of specific PP-InsPs for the AtSPX1-AtPHR1 interaction in yeast. **d** Schematic representation of the PP-InsP biosynthesis pathway in yeast.

Supplementary Fig. 2 Three different AtPHR1 CC crystal structures all share the same tetrameric arrangement.

Structural superposition (shown as C_α traces) of the four-stranded anti-parallel coiled-coil domain of AtPHR1 from crystal forms 1-3.

Supplementary Fig. 3 A conserved dimer- and tetramerization interface in plant MYB CC transcription factors.

a Overview of the AtPHR1 CC dimerization interface. Shown is a ribbon diagram with selected residues contributing to the dimer interface shown in bonds representation. Hydrogen bonds are indicated as dotted lines, residues mutated in the Olig 1 mutants are highlighted in cyan. **b** Overview of the tetramerization interface, with residues mutated in Olig 2 depicted in gold. **c** Structure based sequence alignment of the CC domain of plant MYB CC domain and including a secondary structure assignment calculated with the program DSSP[73]. Residues contributing to the CC dimer interface are shown in blue and cyan, to the tetramerization interface in gold and brown, respectively. The conserved basic residues on the surface of the CC domain are highlighted in magenta.

Supplementary Fig. 4 Growth phenotypes of AtPHR1 CC domain mutants that abolish interaction with AtSPX1 and impact Pi homeostasis.

a Growth phenotype of Col-0 wild type, *phr1-3* , and seedlings of *phr1-3* complementation lines expressing FLAG-AtPHR1, FLAG-AtPHR1^{K325A}, FLAG-AtPHR1^{H328A}, FLAG-AtPHR1^{R335A}, FLAG-AtPHR1$^{K325A\ R335A}$, and FLAG-AtPHR1$^{K325A\ H328A\ R335A}$ under the control of the *AtPHR1* promoter at 14 d after germination (DAG). Seedlings were germinated and grown on vertical $^{1/2}$MS plates for 8 d, transferred to $^{1/2}$MS plates supplemented with either 0 mM, 1 mM or 10 mM Pi and grown for additional 7 d. **b** Growth phenotypes of the

lines in **a**, at 21 DAG. Seedlings were germinated and grown on vertical $^{1/2}$MS plates for eight days, transferred to soil and grown for additional 14 d.

Supplementary Fig. 5 Mutations in the AtPHR1 KHR motif result in Pi hyperaccumulation. **a** Expression of *PHR1* in Col-0, *phr1-3*, and seedlings of *phr1-3* complementation lines expressing FLAG-AtPHR1, FLAG-AtPHR1^{K325A}, FLAG-AtPHR1^{H328A}, FLAG-AtPHR1^{R335A}, FLAG-AtPHR1$^{K325A\ R335A}$, and FLAG-AtPHR1$^{K325A\ H328A\ R335A}$ under the control of the *AtPHR1* promoter relative to the housekeeping gene *Actin2* at 14 DAG. Seedlings were germinated and grown on vertical $^{1/2}$MS plates for 8 d, transferred to $^{1/2}$MS plates supplemented with 1 mM Pi and grown for additional 7 d. For each line, three biological replicates were analysed in technical triplicates by qRT-PCR. Stars indicate significant differences to Col-0 (Dunnett's Test with Bonferroni correction; *, $p < 0.05$). **b-d** Pi content of Col-0 wild type, *phr1-3* seedlings and seedlings of *phr1-3* complementation lines described in **a**. Seedlings were germinated and grown on vertical $^{1/2}$MS plates for 8 d, transferred to $^{1/2}$MS plates supplemented with either 0 mM (b), 1 mM (c) or 10 mM (d) Pi and grown for additional 7 d. For each line, 4 plants were measured in technical duplicates. (*, $p < 0.5$; **, $p < 0.05$).

Supplementary Fig. 6 Mutation in the KHR motif reduces AtPHR1 binding to AtSPX1 in Arabidopsis.

Co-immunoprecipitation experiments using FLAG-tagged wild type and mutant AtPHR1 variants stably expressed in Arabidopsis under the control of the *AtPHR1* promoter. Total protein was extracted from *phr1-3* complementation lines at 10 DAG. Seedlings were germinated and grown on vertical $^{1/2}$MS plates supplemented with 1 mM Pi. FLAG-tag fusions were affinity bound with magnetic FLAG-tag trap, and immunoprecipitation of

1006 FLAG-AtPHR1 was monitored by immunoblot with an anti-FLAG antibody. Co-enrichment

1007 of endogenous AtSPX1 was monitored by immunoblot with an anti-SPX1 antibody.

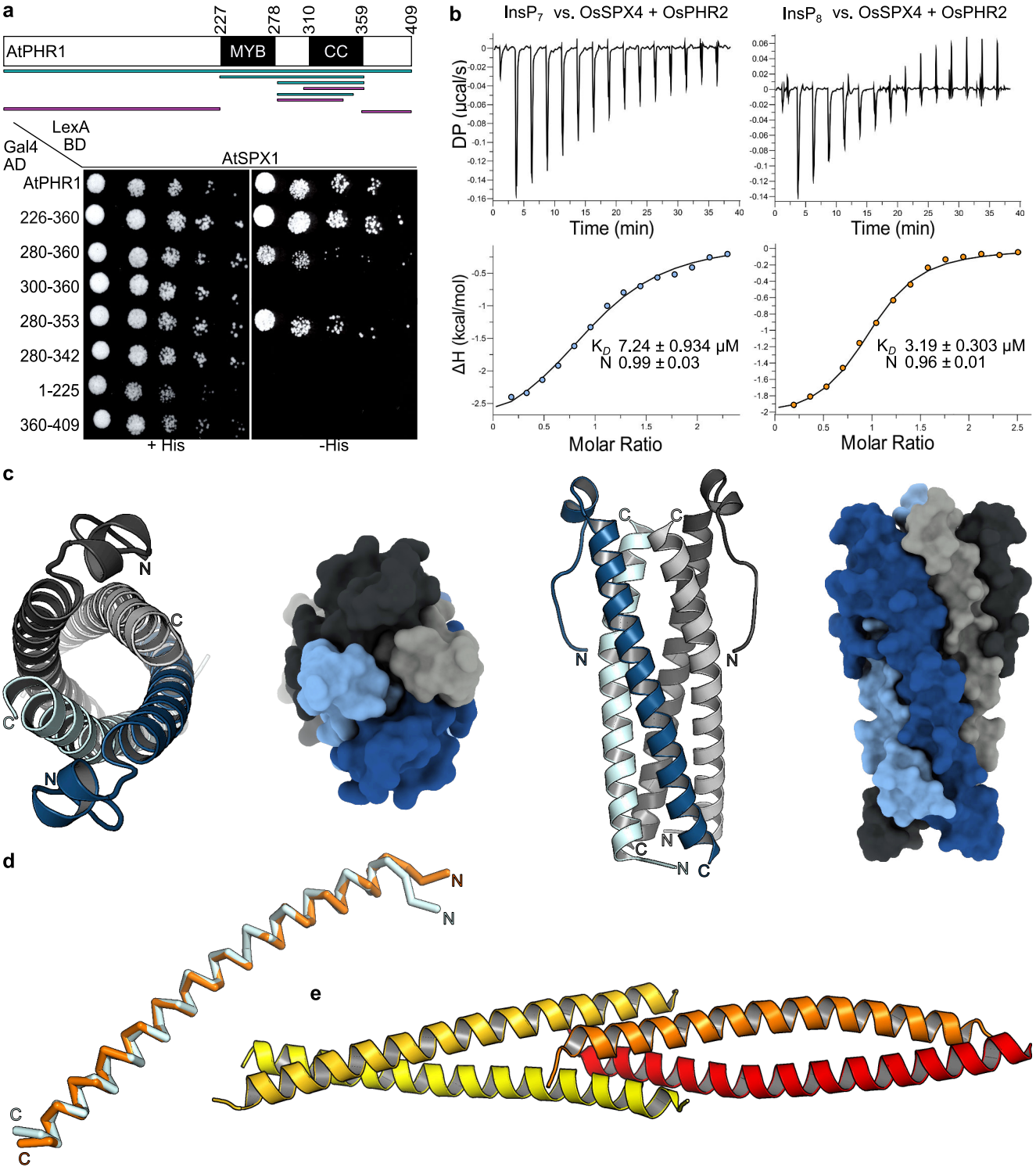

Fig. 1 AtSPX1 recognizes the AtPHR1 CC domain that crystallizes as a tetramer.

a Yeast co-expressing different AtPHR1 deletion constructs fused to the Gal4-activation domain (AD; prey) and full-length wild-type AtSPX1 fused to the LexA-binding domain (BD; bait) were grown on selective SD medium supplemented with histidine (+ His; co-transformation control) or lacking histidine (- His; interaction assay) to map a minimal fragment of AtPHR1 sufficient for interaction with AtSPX1. Shown are serial dilutions from left to right. A schematic overview of the tested interacting (in cyan) and non-interacting (in magenta) AtPHR1 fragments is shown alongside (MYB, DNA binding domain; CC, coiled-coil domain). **b** Isothermal titration calorimetry assays of $InsP_7$ (400 μM 5PP-$InsP_5$; left panel) and $InsP_8$ (500 μM 1,5$(PP)_2$-$InsP_4$; right panel) binding to OsSPX4 – OsPHR2 (30 μM), respectively. Raw heats per injection are shown in the top panel, the bottom panel represents the integrated heats of each injection, fitted to a one-site binding model (solid line). The insets show the dissociation constant (K_d) and binding stoichiometry (N) (± fitting error). **c** Ribbon and surface diagrams of the AtPHR1 CC four-stranded anti-parallel tetramer. Helices contributing to the dimer interface are shown in light- and dark-blue, respectively. Corresponding, symmetry-related helices completing the tetramer are shown in light and dark-grey. **d** Structural superposition of two core CC helices from AtPHR1 (C_α trace, in light blue) and ScCtp1 (PDB-ID 4X01, in orange)[47]. R.m.s.d. is ~1 Å comparing 45 corresponding C_α atoms. **e** Ribbon diagram of the ScCtp1 dimer-of-dimers CC domain, with contributing helices colored from yellow to red.

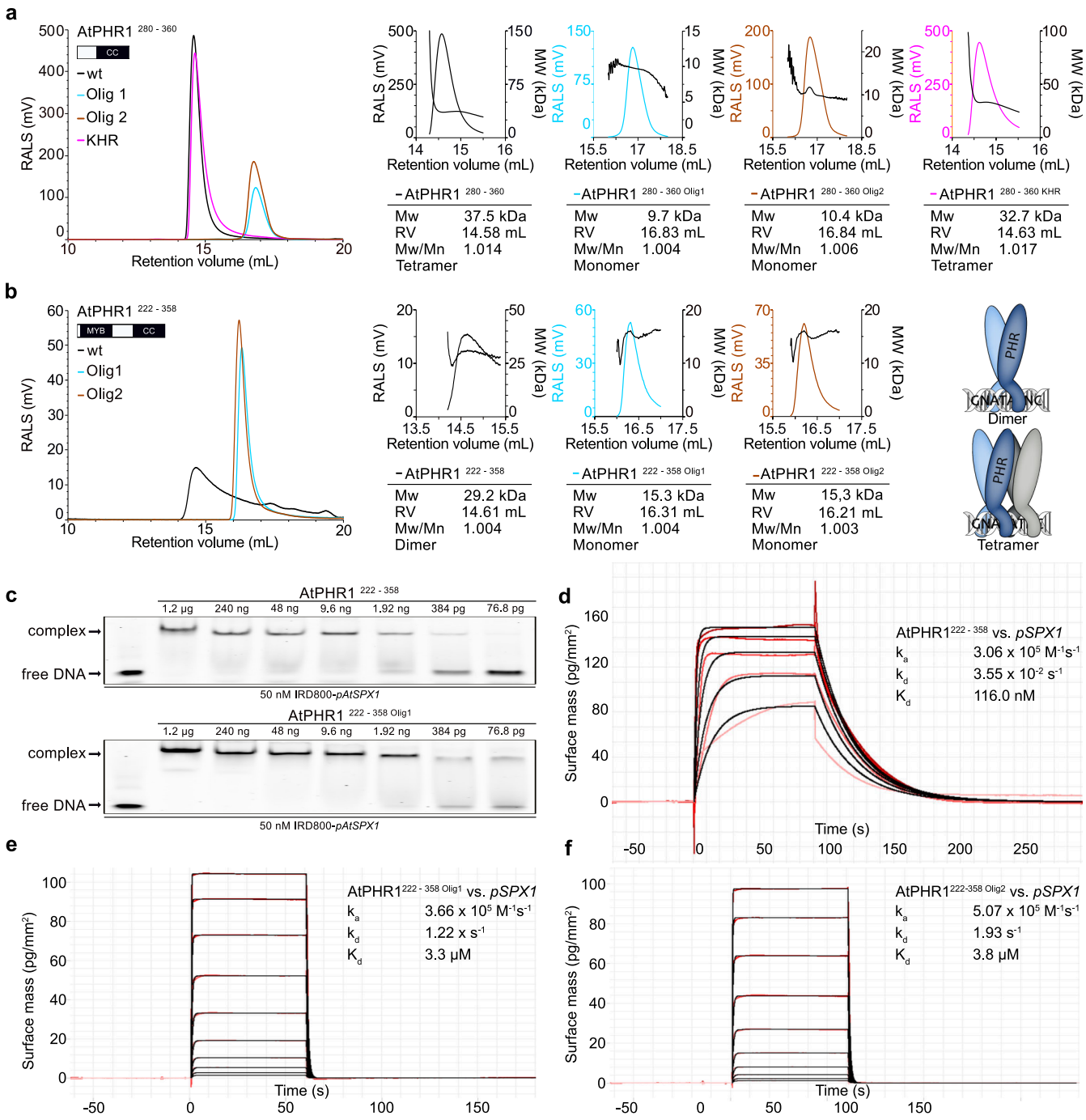

Fig. 2 Mutations in the AtPHR1 CC domain impair oligomerisation and DNA binding.

a Analytical size exclusion chromatography traces of wild type AtPHR1 CC (wt, black line), AtPHR1$^{280-360\ Olig1}$ (Olig 1, cyan), AtPHR1$^{280-360\ Olig2}$ (Olig 2, orange), and of AtPHR1$^{280-360\ KHR}$ (KHR, magenta). The corresponding right-angle light scattering (RALS) traces are shown alongside, the molecular masses are depicted by a black line. Table summaries provide the molecular weight (Mw), retention volume (RV), dispersity (Mw/Mn), and the derived oligomeric state of the respective sample. **b** Analysis of AtPHR1 MYB CC (AtPHR1$^{222-358}$) as described in **a**. **c** Qualitative comparison of the interaction of AtPHR1$^{222-358}$ (upper panel) or AtPHR1$^{222-358\ Olig1}$ (lower panel) binding to IRD800-*pAtSPX1* in electrophoretic mobility shift assays. **d-f**, Quantitative comparison of the interaction of AtPHR1$^{222-358}$, AtPHR1$^{222-358\ Olig1}$, or AtPHR1$^{222-358\ Olig2}$ with *pSPX1* by grating-coupled interferometry (GCI). Sensorgrams show raw data (red lines) and their respective fits (black lines). Table summaries provide the derived association rate (k_a), the dissociation rate (k_d) and the dissociation constant (K_d).

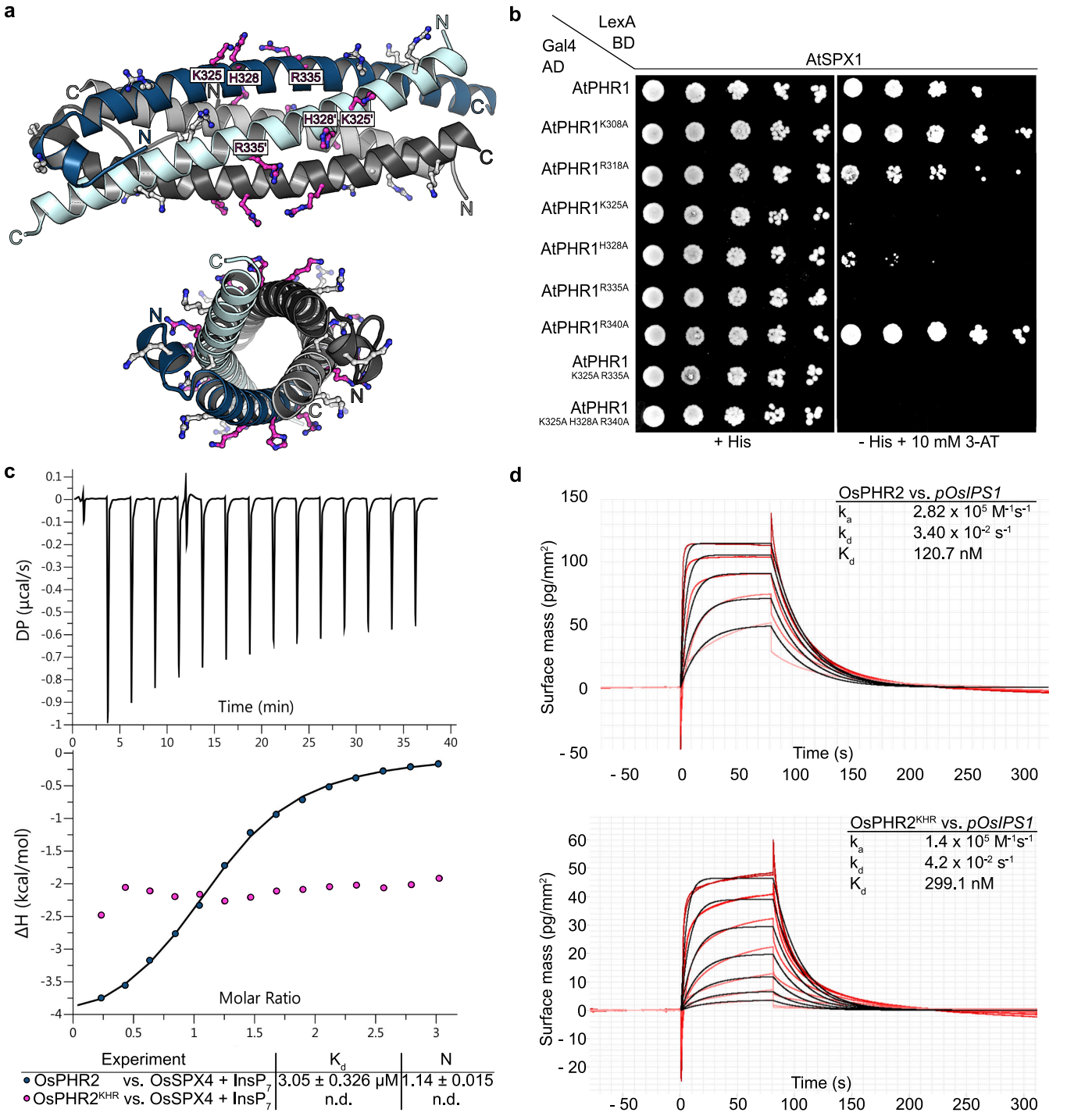

Fig. 3 The KHR motif at the surface of the PHR CC is required for the interaction with SPX domains.
a Ribbon diagram of the AtPHR1 CC domain with conserved basic residues located at the surface of the domain shown in bonds representation. The KHR motif (AtSPX1^{K325}, AtSPX1^{H328}, AtSPX1^{R335}) is highlighted in magenta. **b** Mutational analysis of the basic residues in AtPHR1 CC. Yeast co-expressing AtPHR1$^{226-360}$ variants in which surface exposed basic residues have been replaced with alanine fused to the Gal4-AD (prey) and AtSPX1 fused to the LexA-BD (bait) were grown on selective SD medium supplemented with histidine (+ His; co-transformation control) or lacking histidine and supplemented with 10 mM 3-amini-1,2,4-triazole (3-AT) (- His + 10 mM 3-AT; interaction assay) to identify residues required for interaction with AtSPX1 in yeast two-hybrid assays. Shown are serial dilutions from lift to right. **c** Isothermal titration calorimetry (ITC) assay of wild-type OsPHR2 and OsPHR2^{KHR} (300 µM) versus OsSPX4 (20 µM) - 5PP-InsP$_5$ (100 µM). Raw heats per injection are shown in the top panel, the bottom panel represents the integrated heats of each injection, fitted to a one-site binding model (solid line). The insets show the dissociation constant (K_d) and binding stoichiometry (N) (± fitting error, n.d. no detectable binding). **d** Quantitative comparison of the interaction of OsPHR2 (top panel) or OsPHR2^{KHR} (bottom panel) with *pOsIPS1* by GCI. Sensorgrams show raw data (red lines) and their respective fits (black lines). The insets show summarize association rates (k_a), dissociation rates (k_d) and the dissociation constant (K_d) of the respective sample.

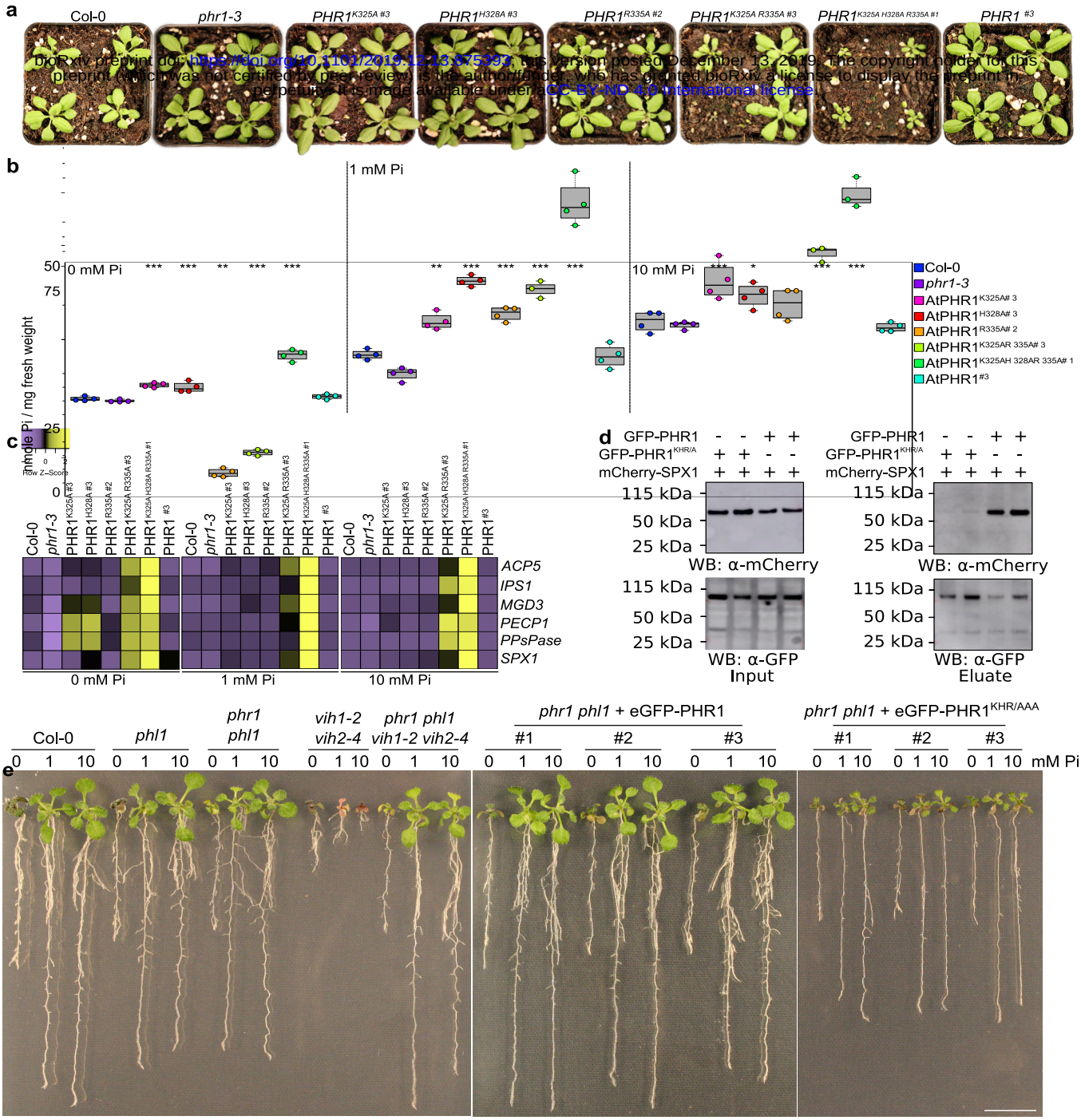

Fig. 4 Mutation of the AtPHR1 KHR motif impairs interaction with AtSPX1 and Pi homeostasis *in planta*. **a** Growth phenotypes of Col-0 wild type, *phr1-3* of *phr1-3* complementation lines expressing FLAG-AtPHR1, FLAG-AtPHR1^{K325A}, FLAG-AtPHR1^{H328A}, FLAG-AtPHR1^{R335A}, FLAG-AtPHR1$^{K325A\ R335A}$, and FLAG-AtPHR1$^{K325A\ H328A\ R335A}$ under the control of the *AtPHR1* promoter at 21 DAG grown in Pi sufficient conditions. One representative line per complementation construct is shown (specified by a #), additional lines are shown in Supplementary Fig. 4. **b** Pi content of the lines shown in a. Seedlings were germinated and grown on vertical $^{1/2}$MS plates for 8 d, transferred to $^{1/2}$MS plates supplemented with either 0 mM, 1 mM or 10 mM Pi and grown for additional 7 d. For each line, four plants were measured in technical duplicates. Pi contents of all lines can be found in Supplementary Fig. 4. **c** Heat maps of PSI marker gene (*ACP5*, *IPS1*, *MGD3*, *PECP1*, *PPsPase*, *SPX1*) expression analyses of the lines shown in **a**, represented as Z-scores. For each line, three biological replicates were analysed in technical triplicates by qRT-PCR. **d** Co-immunoprecipitation (Co-IP) experiment assessing the ability for immobilized GFP-AtPHR1 and GFP-AtPHR1$^{KHR/A}$ to interact with mCherry-AtSPX1 in *N. benthamiana*. Input western blots are shown alongside. **e** Genetic interactions in the VIH-PHR signalling pathway. Col-0 wild type and the indicated mutant seedlings were grown on $^{1/2}$MS plates for 7 DAG, transferred to $^{1/2}$MS plates supplemented with either 0 mM, 1 mM or 10 mM Pi and grown for additional 7 d. For complementation analyses, wild-type AtPHR1 or AtPHR1$^{KHR/AAA}$ was expressed as an N-terminal eGFP fusion protein under the control of the *AtPHR1* promoter. **f** Heat maps of PSI marker gene expression for the lines shown in **e**.

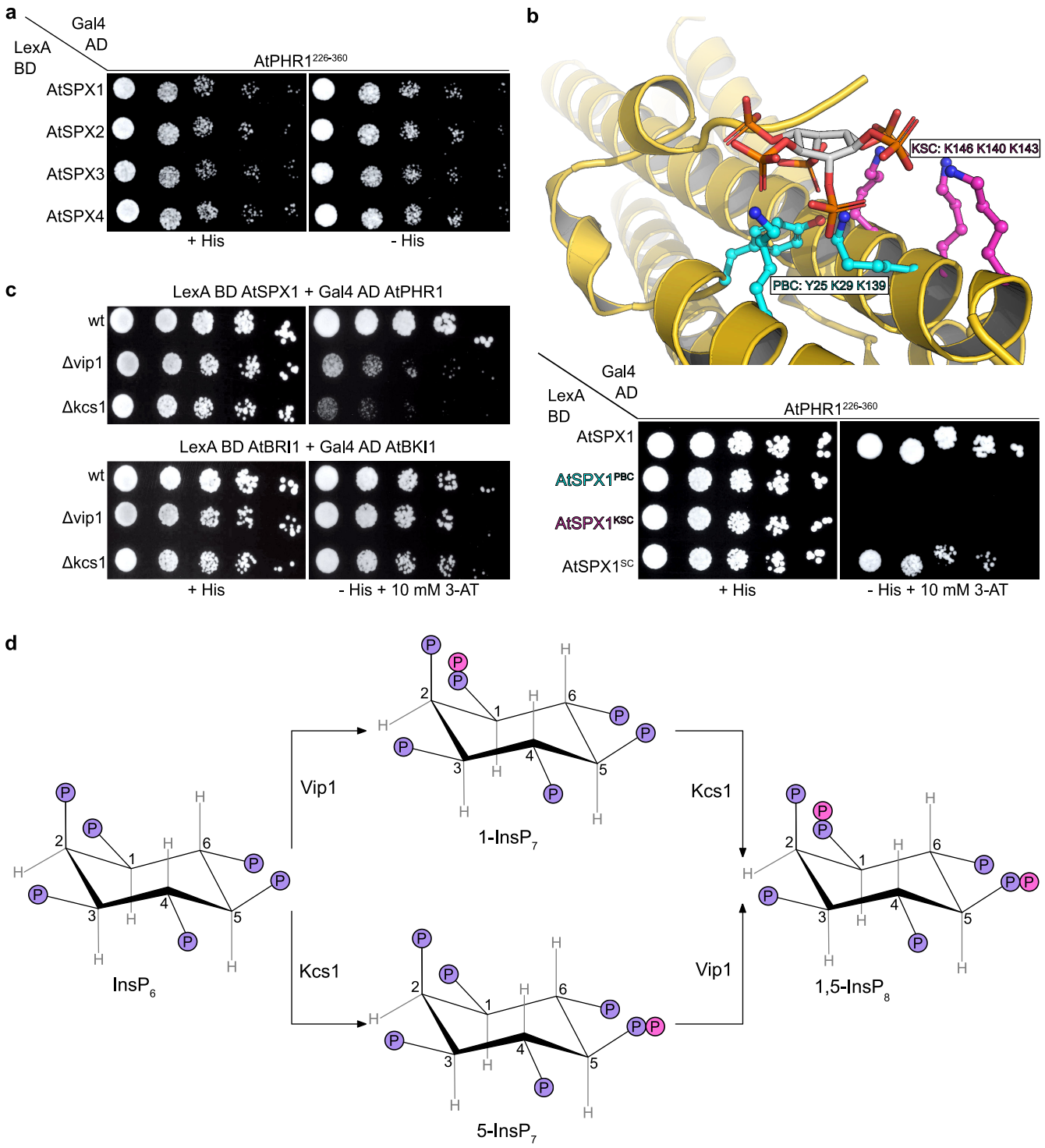

Supplementary Fig. 1 The AtPHR1 – AtSPX1 interaction in yeast is meditated by PP-InsPs.
a Yeast-2-hybrid assay. Yeast co-expressing AtPHR1$^{226\text{-}360}$ fused to the Gal4-AD (prey) and different AtSPX proteins fused to the LexA-BD (bait) were grown on selective SD medium supplemented with histidine (+ His; co-transformation control) or lacking histidine (- His; interaction assay). Shown are serial dilutions from left to right. **b** (Top panel) Homology model of an AtSPX1$^{1\text{-}182}$-InsP$_6$ complex. AtSPX1$^{1\text{-}182}$ is shown as blue ribbon diagram and side chains involved in InsP$_6$ binding are highlighted in green (PBC, phosphate binding cluster) and purple (KSC, lysine surface cluster) and depicted in bonds representation. The InsP$_6$ ligand is shown in grey (in bonds representation). (Bottom panel) Yeast co-expressing AtPHR1$^{226\text{-}360}$ fused to the Gal4-AD (prey) and different AtSPX1 versions mutated in residues involved in InsP$_6$ binding, or a structural control mutant (SC[31]) fused to the LexA-BD (bait) were grown on selective SD medium supplemented with histidine (+ His; co-transformation control) or lacking histidine and supplemented with 10 mM 3-AT(- His + 3-AT; interaction assay) to investigate the importance of the PP-InsP binding surface in AtSPX1 for the AtSPX1 – AtPHR1 interaction in yeast. **c** Yeast knock-out strains for the PP-InsP biosynthesis enzymes Vip1 or Kcs1 co-expressing either AtPHR1$^{226\text{-}360}$ fused to the Gal4-AD (prey) and AtSPX1 fused to the LexA-BD (bait) (upper panel), or AtBKI1 fused to the Gal4-AD (prey) and AtBRI1 fused to the LexA-BD (bait) (lower panel) were grown on selective SD medium supplemented with histidine (+ His; co-transformation control) or lacking histidine and supplemented with 10 mM 3-AT (- His + 3-AT; interaction assay) to investigate the importance of the availability of specific PP-InsPs for the AtSPX1-AtPHR1 interaction in yeast. **d** Schematic representation of the PP-InsP biosynthesis pathway in yeast.

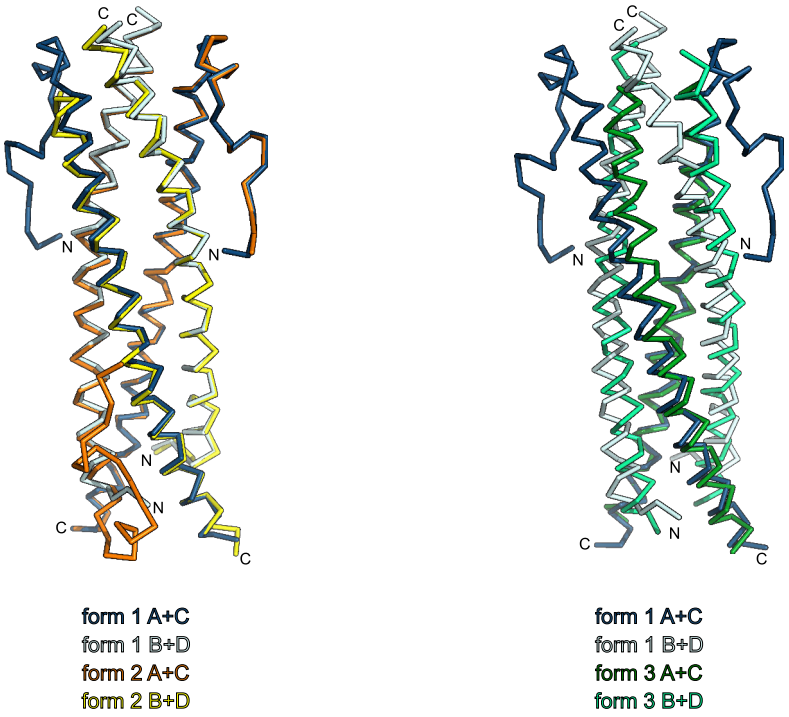

Supplementary Fig. 2 Three different AtPHR1 CC crystal structures all share the same tetrameric arrangement.
Structural superposition (shown as C_α traces) of the four-stranded anti-parallel coiled-coil domain of AtPHR1 from crystal forms 1-3.

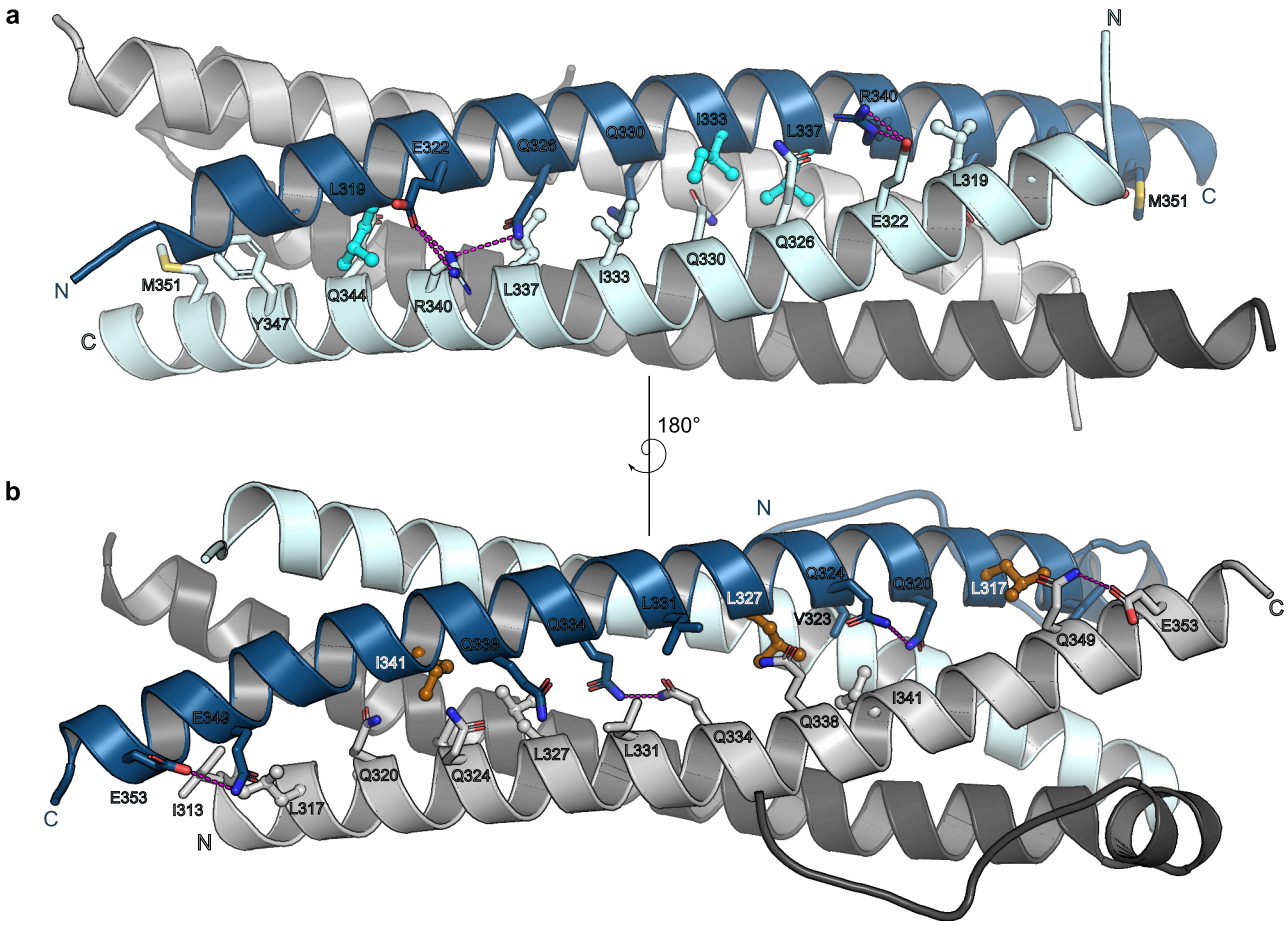

c


```
AtPHR1    PERKLTP--LEHITSLD-LKG-GIGI-TEALRLQMEVQKQLHEQLEIQRNLQLRIEEQGKYLQMMFEKQNS
OsPHR1    SEGKTQEGKTTDELSLD-LKA-SMDL-TEALRLQMEVQKRLHEQLEIQRKLQLRIEEQGKYLQKMFEKQ-C
OsPHR2    SSEKKAA-SKEDIPSID-LKGGNFDL-TEALRLQLELQKRLHEQLEIQRSLQLRIEEQGKCLQMMLEQQ-C
AtPHL1    PQEKKMT-SIEDIKSLD-MKT-SVEI-TQALRLQMEVQKRLHEQLEIQRSLQLQIEKQGRYLQMMFEKQQK
AtPHL2    TGSSSTS-SMRMAQ-QE-QNE-GYQV-TEALRAQMEVQRRLHDQLEVQRRLQLRIEAQGKYLQSILEKA-C
AtPHL3    TGSSSTS-SLRLAA-QE-QNE-SYQV-TEALRAQMEVQRRLHEQLEVQRRLQLRIEAQGKYLQSILEKA-C
AtPHL4    PEARLTP--LEQITSDD-TKR-GIDI-TETLRIQMEHQKKLHEQLESLRTMQLRIEEQGKALLMMIEKQNM
AtPHL5    GKFEKRA-CAKELSQLD-TRT-GVQI-KEALQLQLDVQRHLHEQLEIQRNLQLRIEEQGKQLKMMMEQQQK
AtPHL6    SEEKKLA-LSKSEADEK-KKG-AIQL-TEALRMQMEVQKQLHEQLEVQRVLQLRIEEHAKYLEKMLEEQRK
AtPHL7    KKTDKKE-SGDMLSGLD-GSS-GMQI-TEALKLQMEVQKRLHEQLEVQRQLQLRIEAQGKYLKKIIEEQ-Q
AtPHL8    SRDLRGC-SVTEENSNP-AKE-GLQI-TEALQMQMEVQKKLHEQIEVQRHLQVKIEAQGKYLQSVLMKA-Q
AtPHL11   SQGGISN-DSRFDNHQR-QSG-NVPF-AEAMRHQVDAQQRFQEQLEVQKKLQMRMEAQGKYLLTLLEKAQK
AtPHL12   RDTNRAS-MLDLRRNAVFTTS-PLIIGRNMNEMQMEVQRRIEEEVVIERQVNQRIAAQGKYMESMLEKA-C
AtPHL13   PLVKNLK-TIEDIKSLD-LKT-SIEI-TEALRLQMKVQKQLHEQLEIQRSLQLQIEEQGRYLQMMIEKQQK
AtMYR1    PEVDESH-SESLSIGPQ-PSM-NLPI-SDALQMQIEVQRRLHEQLEVQRHLQLRIEAQGKYLQSILEKA-Q
AtMYR2    PDADEIQ-SENLSIGPQ-PNK-NSPI-GEALQMQIEVQRRLHEQLEVQRHLQLRIEAQGKYLQSVLEK---
AtWDY     KEGSRAS-AMDIQRNVA-SSS-GMMS-RNMNEMQMEVQRRLHEQLEVQRHLQLRIEAQGKYMQSILERA-C
                              L317 L319      L327      I333 L337      I341
                                             K325 K328      K335
```

Supplementary Fig. 3 A conserved dimer- and tetramerization interface in plant MYB CC transcription factors.
a Overview of the AtPHR1 CC dimerization interface. Shown is a ribbon diagram with selected residues contributing to the dimer interface shown in bonds representation. Hydrogen bonds are indicated as dotted lines, residues mutated in the Olig 1 mutants are highlighted in cyan. **b** Overview of the tetramerization interface, with residues mutated in Olig 2 depicted in gold. **c** Structure based sequence alignment of the CC domain of plant MYB CC domain and including a secondary structure assignment calculated with the program DSSP[73]. Residues contributing to the CC dimer interface are shown in blue and cyan, to the tetramerization interface in gold and brown, respectively. The conserved basic residues on the surface of the CC domain are highlighted in magenta.

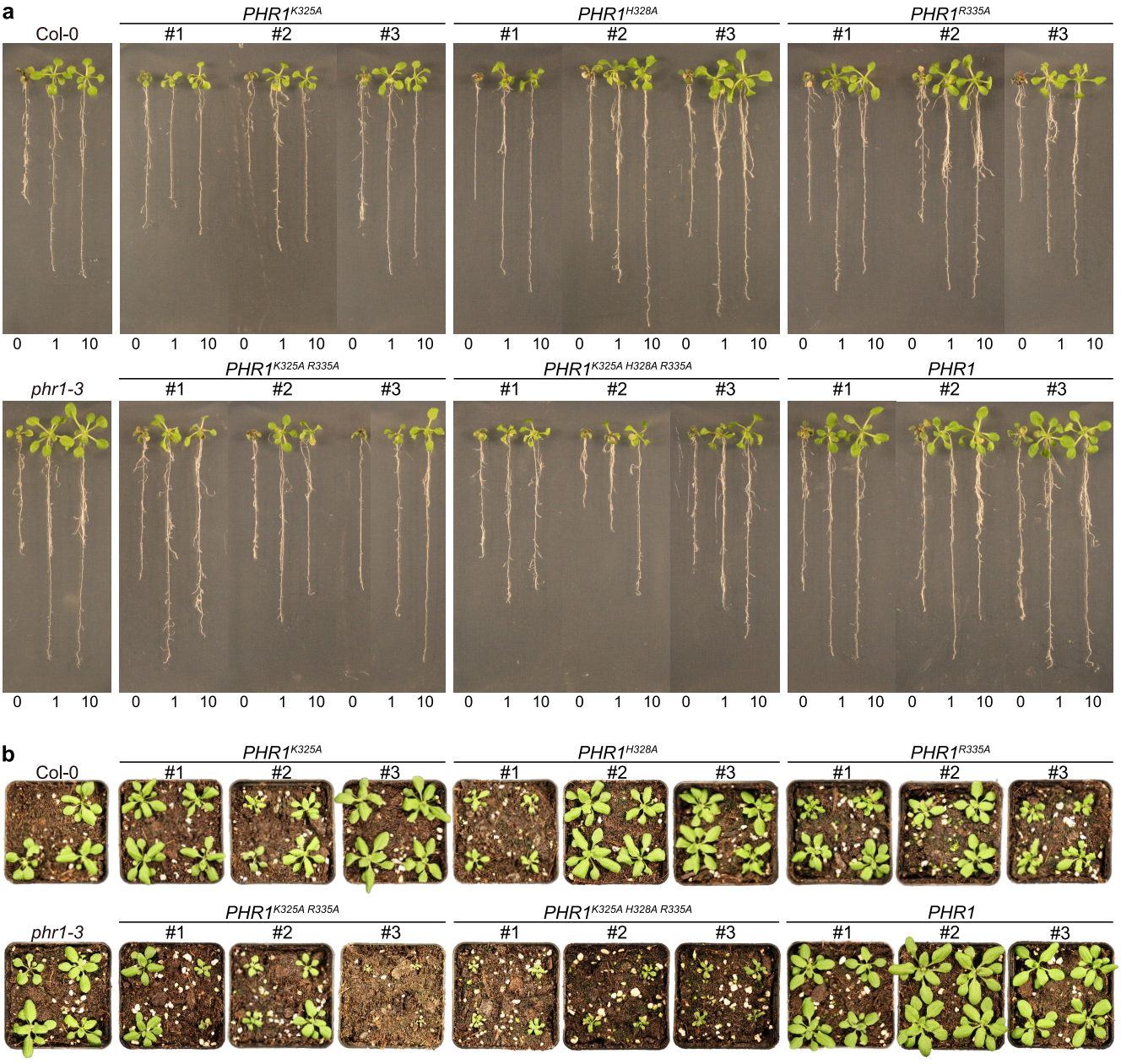

Supplementary Fig. 4 Growth phenotypes of AtPHR1 CC domain mutants that abolish interaction with AtSPX1 and impact Pi homeostasis.
a Growth phenotype of Col-0 wild type, *phr1-3* , and seedlings of *phr1-3* complementation lines expressing FLAG-AtPHR1, FLAG-AtPHR1^{K325A}, FLAG-AtPHR1^{H328A}, FLAG-AtPHR1^{R335A}, FLAG-AtPHR1$^{K325A\ R335A}$, and FLAG-AtPHR1$^{K325A\ H328A\ R335A}$ under the control of the *AtPHR1* promoter at 14 d after germination (DAG). Seedlings were germinated and grown on vertical $^{1/2}$MS plates for 8 d, transferred to $^{1/2}$MS plates supplemented with either 0 mM, 1 mM or 10 mM Pi and grown for additional 7 d. **b** Growth phenotypes of the lines in **a**, at 21 DAG. Seedlings were germinated and grown on vertical $^{1/2}$MS plates for eight days, transferred to soil and grown for additional 14 d.

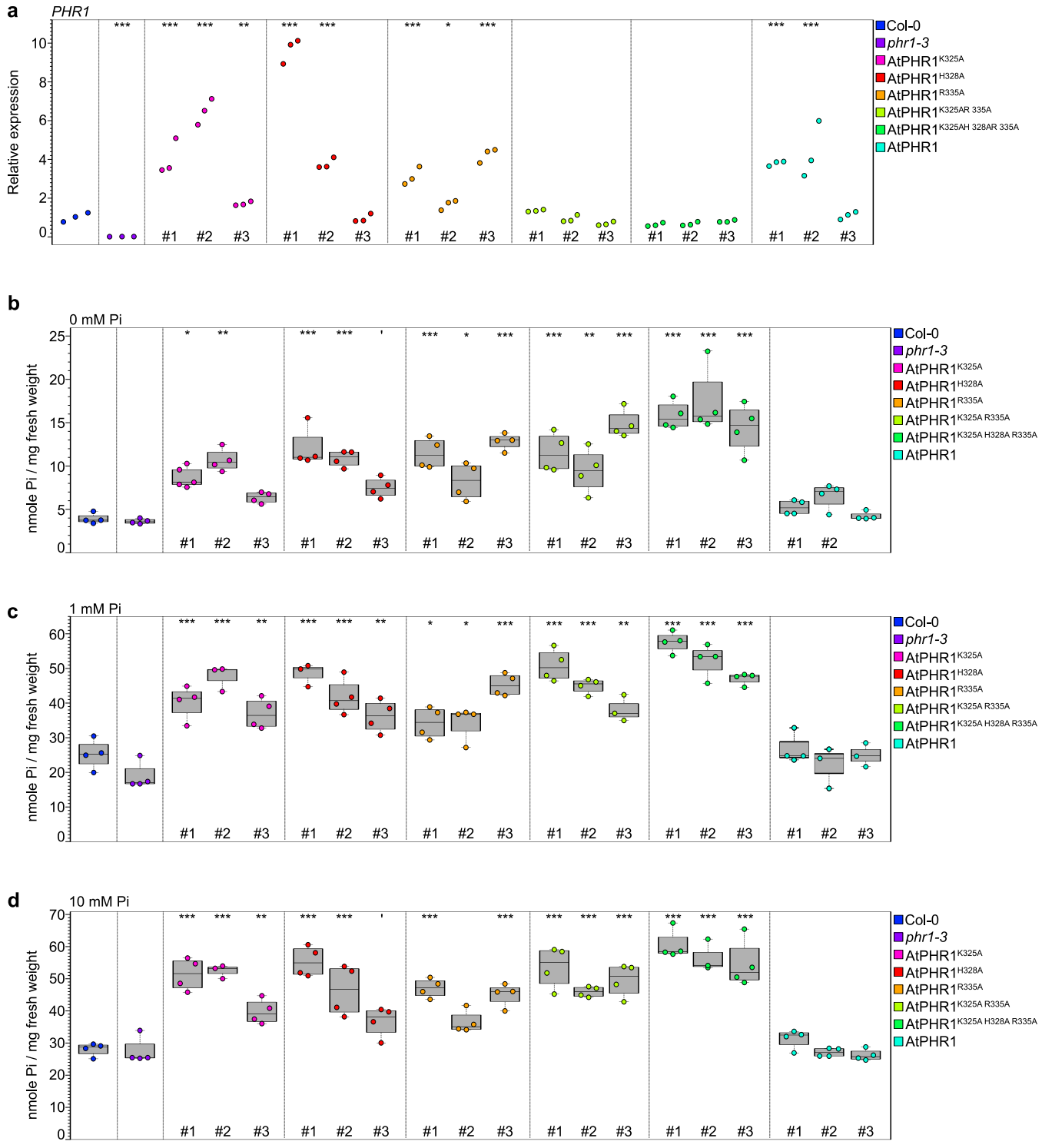

Supplementary Fig. 5 Mutations in the AtPHR1 KHR motif result in Pi hyperaccumulation.

a Expression of *PHR1* in Col-0, *phr1-3*, and seedlings of *phr1-3* complementation lines expressing FLAG-AtPHR1, FLAG-AtPHR1^{K325A}, FLAG-AtPHR1^{H328A}, FLAG-AtPHR1^{R335A}, FLAG-AtPHR1$^{K325A\ R335A}$, and FLAG-AtPHR1$^{K325A\ H328A\ R335A}$ under the control of the *AtPHR1* promoter relative to the housekeeping gene *Actin2* at 14 DAG. Seedlings were germinated and grown on vertical $^{1/2}$MS plates for 8 d, transferred to $^{1/2}$MS plates supplemented with 1 mM Pi and grown for additional 7 d. For each line, three biological replicates were analysed in technical triplicates by qRT-PCR. Stars indicate significant differences to Col-0 (Dunnett's Test with Bonferroni correction; *, $p < 0.05$). **b-d** Pi content of Col-0 wild type, *phr1-3* seedlings and seedlings of *phr1-3* complementation lines described in **a**. Seedlings were germinated and grown on vertical $^{1/2}$MS plates for 8 d, transferred to $^{1/2}$MS plates supplemented with either 0 mM (b), 1 mM (c) or 10 mM (d) Pi and grown for additional 7 d. For each line, 4 plants were measured in technical duplicates. (*, $p < 0.5$; **, $p < 0.05$).

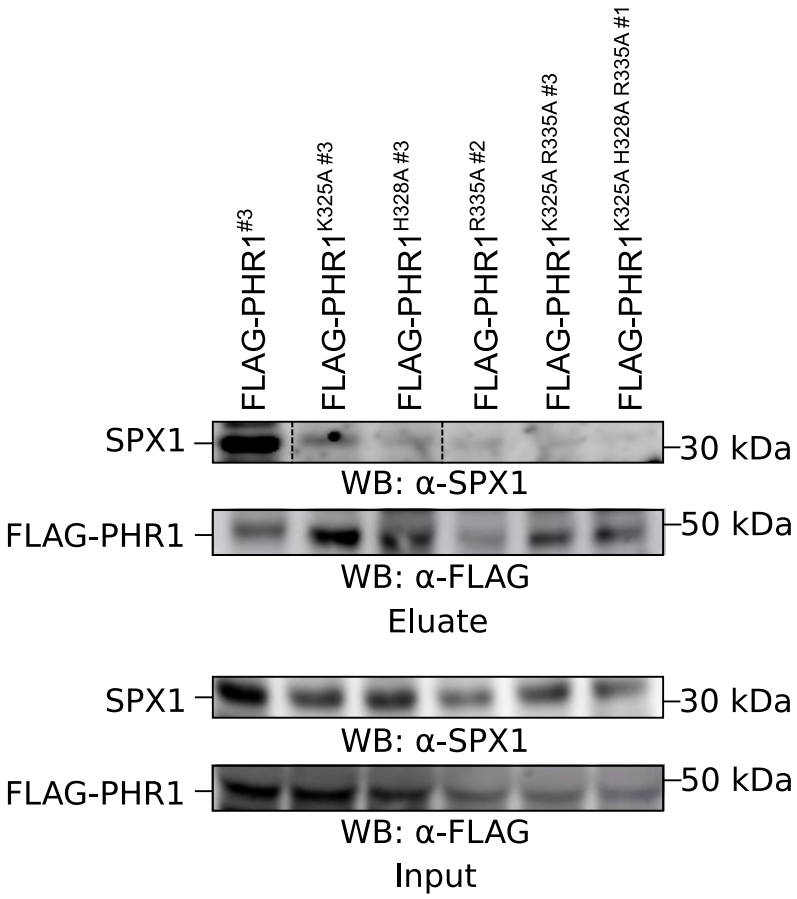

Supplementary Fig. 6 Mutation in the KHR motif reduces AtPHR1 binding to AtSPX1 in Arabidopsis.
Co-immunoprecipitation experiments using FLAG-tagged wild type and mutant AtPHR1 variants stably expressed in Arabidopsis under the control of the *AtPHR1* promoter. Total protein was extracted from *phr1-3* complementation lines at 10 DAG. Seedlings were germinated and grown on vertical $^{1/2}$MS plates supplemented with 1 mM Pi. FLAG-tag fusions were affinity bound with magnetic FLAG-tag trap, and immunoprecipitation of FLAG-AtPHR1 was monitored by immunoblot with an anti-FLAG antibody. Co-enrichment of endogenous AtSPX1 was monitored by immunoblot with an anti-SPX1 antibody.